The Pennsylvania State University

The Graduate School

College of Engineering

COHERENT OMNIPRESENT FLUCTUATIONS IN THE IONOSPHERE

A Dissertation in

Electrical Engineering

By

Dorey Joseph Livneh

Submitted in Partial Fulfillment
of the Requirements
for the degree of

Doctor of Philosophy

May 2009

The dissertation of Dorey J. Livneh was reviewed and approved* by the following:

John D. Mathews
Professor of Electrical Engineering
Dissertation Adviser
Chair of Committee

Victor Pasko
Professor of Electrical Engineering

C. Russell Philbrick
Professor of Electrical Engineering

Hampton N. Shirer
Associate Professor of Meteorology

W. Kenneth Jenkins
Professor of Electrical Engineering
Head of the Department of Electrical Engineering

*Signatures are on file in the Graduate School

Abstract

Incoherent Scatter Radar power observations at Arecibo, Millstone Hill, and the Poker Flat AMISR have revealed the continuous presence of Coherent Omnipresent Fluctuations in the Ionosphere (COFIs) with periods ranging from roughly 30 to 60 minutes and apparent vertical wavelengths increasing with altitude from tens to hundreds of km. Upon high-pass filtering of the radar power profile and electron concentration data, the COFIs are seen unambiguously and ubiquitously in Arecibo results from 22-23 March 2004, 5-6 June, 21-25 September, and 17-20 November 2005, as well as in Millstone Hill results from 4 October to 4 November 2002. The COFIs are strong throughout the F-region, often spanning altitudes of 160 km to above 500 km, and are detected day and night in the F2-layer (above ~ 200 km). In fact, the COFIs are seen at every time and altitude that there is sufficient plasma to produce a radar echo. The COFIs also are observed at Poker Flat, although the poor signal-to-noise ratio over segments of the data makes it difficult to determine whether or not they are always present. The consistent detection of the COFIs, along with the longitudinal alignment and large latitudinal spread of the observation sites suggests that these waves always are present over at least a major portion of the northern hemisphere.

This phenomenon appears to have been reported in Total Electron Concentration (TEC) maps of the ionosphere over much of North America as well as in airglow images from Arecibo and many other mid-latitude sites around the world. These observations give us insight into the horizontal properties of the waves. Although Medium Scale Traveling Ionospheric Disturbances (MSTIDs) generally are associated with aurorally generated acoustic-gravity waves (AGWs), the properties of the COFIs may suggest otherwise.

Other possible source mechanisms are presented; notably a possible link to oscillations in the solar wind and magnetosphere is described. Consistent fluctuations with periods of about an hour have been observed in magnetic field measurements taken at geosynchronous altitudes by the Geostationary Operational Environmental Satellites (GOES)-10 and -12 satellites that may be linked to the COFIs. Concurrent solar wind data from ACE are presented in an attempt to find a more primary source of the COFIs. Both the AGW and magnetospheric explanations for the COFIs are discussed, along with arguments for and against each scenario.

Table of Contents

List of Figures

List of Tables

Acknowledgements

This thesis was completed with the help of some outstanding people who deserve my thanks. My parents, Steve and Deborah, have been great examples and have given me constant support, advice, and patience throughout my life and the duration of this project. They have been wonderful parents and did the best they could with me given my limitations. My grandfather, David has helped me throughout my academic career with financial and psychological support and is an all around good guy. I'd also like to thank my brother, Ben so he doesn't feel left out.

Dr. John D. Mathews has really been an excellent advisor, scientific role model, and a constant fountain of good ideas and even better puns. He's been easily my favorite 'boss' of all time and I'm not just saying that because I hope to graduate. I'd like to thank my committee members. Dr C. Russell Philbrick has provided good counsel and has shared his immense knowledge of space and geo-physics. Dr. Victor Pasko helped me understanding the effects of horizontal winds on acoustic-gravity waves. Dr. Hampton N. Shirer has been a positive voice on my committee and endured my previous presentation.

This work couldn't have been completed without my collaborators. Frank T. Djuth has been of enormous assistance; he has been full of ideas which he has shared on my papers. Ilgin Seker and I have collaborated on several papers and he has been instrumental in providing airglow imager observations and information about them.

Three colleagues of mine deserve special mention here. Stanley J. Briczinski helped me get 'up and running' on this project. He taught me how to use a Mac, how to program in IDL, helped with course work and gave me a grounding in electromagnetism. Akshay Malhotra has given me useful feedback and has shared his enthusiastic approach to science. Jonathan B. Snively helped me with many issues including MATLAB, the candidacy exam, and understanding acoustic-gravity waves.

So, that's it. Thanks to everyone. I hope you enjoy reading this as much as I enjoyed writing it. This effort was supported under NSF Grant ATM 07-21613 to the Pennsylvania State University. The Arecibo Observatory is part of the National Astronomy and Ionosphere Center, which is operated by Cornell University under cooperative agreement with the National Science Foundation.

1. Introduction

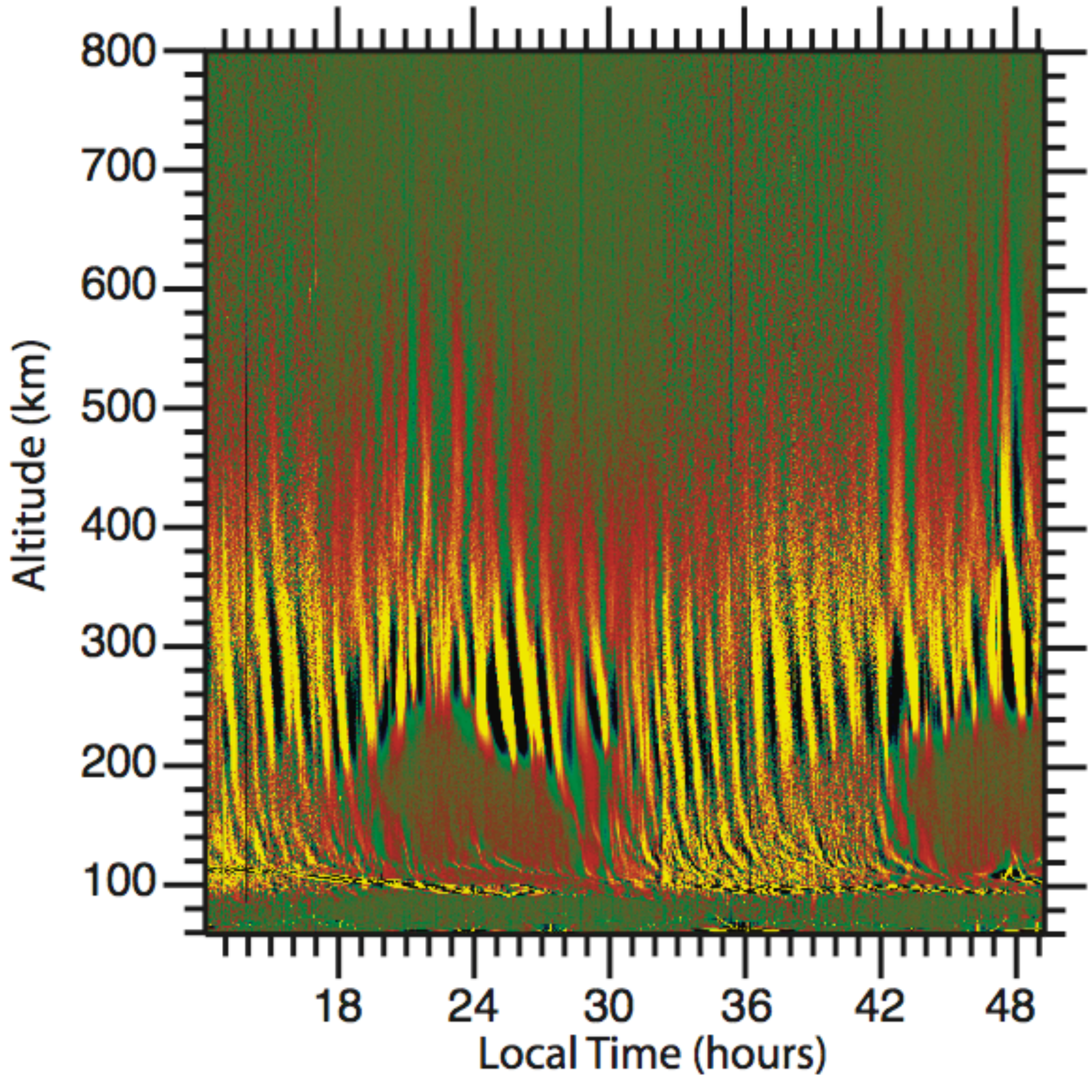

Figure 1.1. Coherent Omnipresent Fluctuations in the Ionosphere (COFIs) as observed at Arecibo on June 5-7, 2005.

In 2005, a close examination of Incoherent-Scatter-Radar (ISR) power profile results from Arecibo Radio Observatory (18.3° North, 66.8° West) revealed faint, vertically coherent quasi-periodic fluctuations in the overhead ionosphere [*Livneh et al.*, 2007]. High-pass filtering of the data sets showed vertically coherent fluctuations with periods of 30-60 minutes and vertical wavelengths increasing with altitude from tens to hundreds of km (e.g. Figure 1.1). Surprisingly, these waves were found to be present *continuously* throughout the entire observable F-region[1], a previously unknown result[2]. Over all nine days (four data sets from three seasons) of available Arecibo power profile data, these waves were present at all times and at all F-region altitudes where there was sufficient signal-to-noise-ratio (SNR) to observe them (130 to ~700 km). One month of electron concentration data from the Millstone Hill Observatory (42.6° North, 71.5° West) also showed consistent evidence of these waves. These waves were later seen much more faintly in electron concentration results from the ISR at Poker Flat, Alaska (65.1° North, 147.4° West).

The literature abounds with reports of Traveling Ionospheric Disturbances (TIDs). The COFIs are certainly a form of TIDs. However, for ease of reference and to distinguish these *ubiquitous* waves from TIDs in general, the waves that are the focus of this dissertation are referred to as Coherent Omnipresent Fluctuations in the Ionosphere (COFIs) throughout this document.

---

[1] The waves are seen everywhere and at all times that the F-region electron concentration is high enough to produce a detectable radar echo.

[2] It is likely that previous researchers did not realize the ubiquity of waves (COFIs) in the ionosphere because the data storage, signal processing, and visualization capabilities required to view them were unattainable until the recent advancements in computing power. An observation of ionospheric oscillations with the vertical coherence and temporal continuity of the COFIs does not appear in the previous literature. However, *Mathews et al.* [2001] likely observed the faint nighttime F1-region trails of the COFIs and gave them the name 'ion rain'. *Djuth et al.* [2004] presaged the finding of the COFIs with their daytime F1-region observations and predicted that gravity waves were routinely present in the thermosphere over Arecibo.

1.1. Background

The subject of this dissertation is Coherent Omnipresent Fluctuations in the Ionosphere (COFIs) in the F-region of the Earth's ionosphere. The nature and possible sources of the COFIs are investigated using a combination of empirical observation and informed conjecture. As this endeavor requires a working knowledge of various concepts in space and geophysics, a brief initiation to the topics that are fundamental to this thesis is provided in the following pages.

1.1.1. The Earth's Atmosphere

Our Earth is enveloped in a layer of gas that we term the atmosphere. The Earth's atmosphere is composed of many constituents, among which N_2 and O_2 are by far the most prevalent. Most of the atmosphere is concentrated near the Earth's surface; atmospheric density to first order decreases exponentially with altitude. In fact, half of the total mass of the atmosphere lies in its lowest 5.5 km, which handily coincides with the Earth's surface that we inhabit. This exponential decrease in density continues so that at F-region heights, say 300 km, the density is some 12 orders of magnitude smaller than at sea level [MSISE-90 model: http://omniweb.gsfc.nasa.gov/vitmo/msis_vitmo.html].

The density and pressure decrease can be derived as follows - after [*Banks and Kockarts,* 1973 pp. 7, 33-35]. For a stable atmosphere, the change in pressure, p, resulting from a change in altitude, z, is equal to the weight of the air lying between the initial height and the new height and we have the *hydrostatic equation*:

$$\rho g = -\frac{dp}{dz} , \tag{1-1}$$

where g is the acceleration due to gravity and ρ is the atmospheric density. To a large extent, the atmosphere obeys the ideal gas law:

$$p = \rho RT = nkT; \tag{1-2}$$

where T is the temperature, R=287 J/kg/K is the gas constant for dry air, n is the molecular concentration or number density and $k = 1.3803 \times 10^{-16}$ erg·deg^{-1} is Boltzmann's constant. Also,

$$\rho = nm. \tag{1-3}$$

Combining (1-2) and (1-3) and solving for ρ:

$$\rho = \left(\frac{m}{kT}\right)p. \tag{1-4}$$

Substituting (1-4) into (1-1) we get:

$$\frac{dp}{dz} = -\left(\frac{mg}{kT}\right)p\ , \tag{1-5}$$

or:

$$\frac{dp}{p} = -\left(\frac{mg}{kT}\right)dz = -\frac{dz}{H(z)} \tag{1-6}$$

Here H is an important atmospheric parameter called the *scale height* which varies with altitude since T, m, and g are all functions of z, $H(z) = kT(z)/m(z)g(z)$. $H(z)$ is the altitude difference over which the pressure changes by a factor of e. Recognizing the left side of (1-6) as the derivative of the logarithm of p and integrating yields:

$$p(z) = p_0 \exp\left[-\int_{z_0}^{z} \frac{dz}{H(z)}\right], \tag{1-7}$$

Simplifying (1-7) requires making assumptions about the variables on which *H(z)* depends. A useful first-order approximation is to assume an isothermal constant gravity, constant composition atmosphere so that *H(z)* is a constant and (1-7) simplifies to:

$$p(z) = p_0 \exp\left[-\frac{z}{H}\right] = p_0 \exp\left[-\left(\frac{mg}{kT}\right)z\right], \qquad \text{(1-8)}$$

thereby exhibiting an exponential decrease of pressure – and density by (1-4) - with altitude in this common approximation.

The Earth's atmosphere is often divided into regions based on temperature variation (see Figure 1.2). Near the Earth's surface, the temperature decreases with height at the moist adiabatic lapse rate of around 6-7°K/km [*Wallace and Hobbs,* 2006, p. 77], in a region known as the troposphere. Due primarily to the absorption of solar UV energy by ozone, this trend reverses at a height of around 12 km and the stratosphere begins, extending up to the stratopause at approximately 50 km altitude[3]. The mesosphere is the next region up, where "vibrational relaxation" of carbon dioxide molecules causes the temperature to decrease with height at a rate of about 3°K/km until the coldest point of the atmosphere (~181°K) is reached at the mesopause, which has a height of around 80 km [*Tascione*, 1994 p. 79]. Above this altitude, the temperature increases with height due to the absorption of solar radiation as soft X-ray, UV and EUV absorption, as well as by Joule heating and particle precipitation in the polar regions [*Kato*, 2007, p. 222], and we find temperatures well in excess of 1000 K during solar maximum conditions in the region known as the thermosphere. It is in the thermosphere

[3] Note that the altitude ranges given here for the atmospheric regions vary strongly with geographic latitude.

and upper mesosphere that the bombardment by the sun's rays creates a charged region known as the ionosphere.

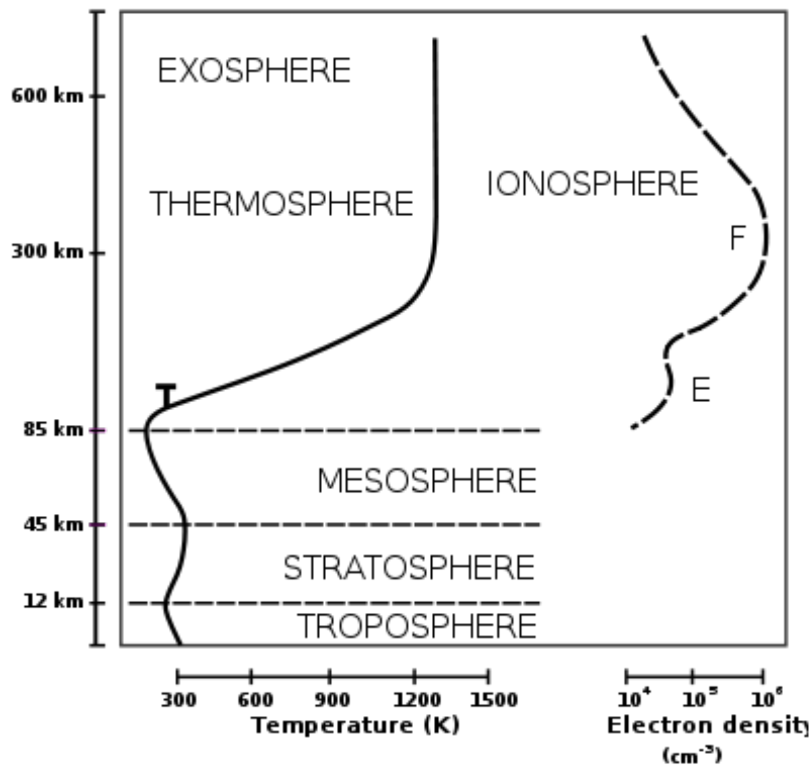

Figure 1.2. A typical vertical temperature profile for the Earth's atmosphere. Notice the changing temperature variation associated with each atmospheric region. From http://www.nationmaster.com/encyclopedia/Ionosphere.

1.1.2. The Ionosphere

When a photon with sufficient energy strikes an appropriate atom or molecule, it may cause the particle to separate or *ionize* into a free electron and a positively charge ion in a process known as *photoionization*. When positive ions and free electrons are present in sufficient number that the electrodynamic forces they exert on one another cause them to act collectively the material is termed a *plasma*. In contrast to a plasma which exhibits a response to Coulombic forces, magnetic fields, and the motion of the background gas, the particles of a neutral gas only affect each other through collisions and do not exhibit collective behavior. Thus, a plasma is a group of charged particles whose electrodynamic forces on each other cause them to exhibit collective behavior. On the sunlit side of the Earth, photons coming from the sun photoionize large numbers of particles, creating the plasma of the ionosphere. Essentially, the ionosphere is a layer of partially ionized atmosphere beginning at around 70 km above the Earth's surface and extending outwards into space. The ionosphere does not play a significant role in the lower atmosphere because most of the photons of sufficient energy to ionize particles (EUV) are absorbed in the upper atmosphere. The few energetic photons that survive the journey through the upper atmosphere encounter an exponentially increasing number of neutral particles, limiting their relative effects. Hard x-rays generate the D-region (below 90 km) in the daytime.

Even in the ionosphere, the neutral density far exceeds that of the plasma. Only at altitudes of several thousand kilometers does the plasma density begin to rival that of the neutrals [*Kelley*, 1989 p. 23]. The peak plasma concentration (number density) of about 10^6 [*Tascione*, 1994, p. 92] occurs around noon at an altitude of roughly 300 km - at the peak of the F2-layer. A note on terminology - a *layer* is plasma in higher concentration than in the areas above and below; while a *region* is the area occupied by the layer, i.e. the F-layer is in the F-region. The F2 layer is the upper part of the F-layer, which also includes the F1-layer that peaks at ~160 km during the daytime as this is the photoionization peak. The F2-layer is composed of atomic oxygen ions that have much lower recombination rates, which, along with the large mean free path at F2-region heights making opportunities for recombination less frequent, allow it to survive the absence of sunlight. In contrast, the F1-layer nearly disappears at night due to the lack of photoionization and the higher ion-electron recombination rates of its molecular ion constituents, NO^+, and O_2^+. Below the F-layer is the E-layer which is also largely curtailed at night as it too is composed of NO^+, and O_2^+ and spans the altitudes between roughly 90 and 150 km [*Kelley*, 1989, pp. 6-7]. An altitude thin layer of metallic ions called the 'Sporadic-E' does tend to remain in place of the larger E-region at night e.g. [*Mathews*, 1998]. Below the E-region lies the D-region that although important, is not relevant to the present study.

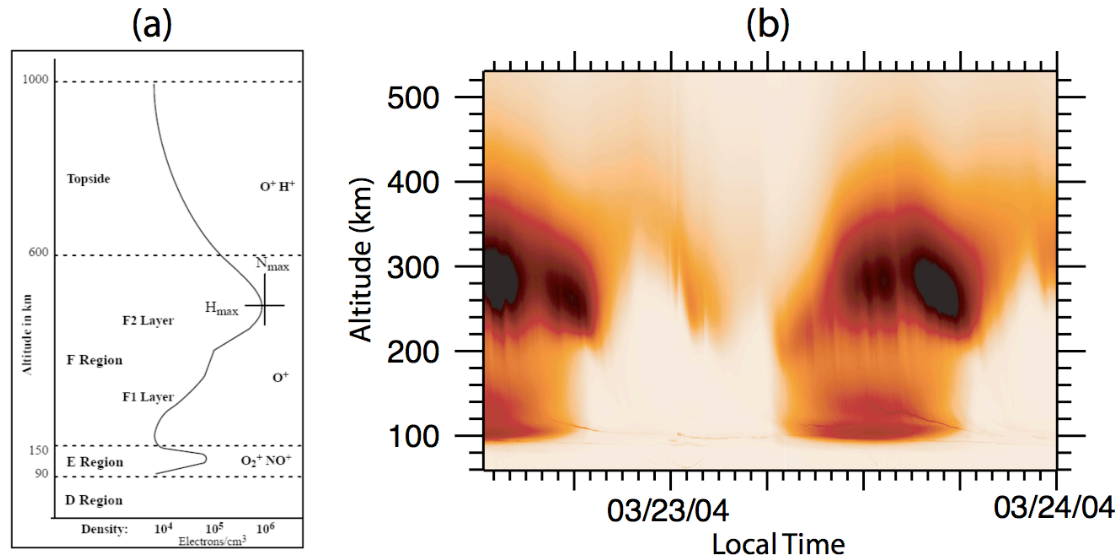

Figure 1.3. (a) A typical vertical electron concentration profile of the ionosphere taken from http://commons.wikimedia.org/wiki/File:IonosphereProfileNOAA.png. The E- and F-regions of the ionosphere on March 22-24, 2004. This plot shows how the vertical electron concentration profiles evolve with time through a typical quiet day. The darker areas indicate higher electron concentration. The F-2 layer (above ~200 km) is present day and night but the F-1 (below ~200 km) vanishes due to its higher recombination rates and lack of production at night.

1.1.3. Acoustic-Gravity Waves (AGWs)

Suppose that a parcel of air is displaced upwards from its equilibrium position and finds itself to be of greater density than the air that now surrounds it, experiences a downward force and falls beyond its starting position, finds itself lighter than the surrounding air and is sent back upwards by the buoyancy force; thus resulting in an oscillation that continues due to the dueling forces of gravity and buoyancy. It is this mechanism that is responsible for acoustic-gravity waves. Of course, an initial downward displacement of the air parcel would still cause the gravity wave to form. The maximum frequency that an acoustic gravity can attain is called the Brunt-Väisälä frequency. This frequency is only achieved for purely vertical air parcel displacements.

If the air parcel motion also has a horizontal component then the wave frequency decreases. Gravity waves are a part of that spectrum of waves associated with pressure disturbances acting on the atmospheric gases. Acoustical waves, or sound waves, are always excited by sources in supersonic motion and travel as longitudinal compression waves at the speed of sound in the medium. Beyond the low frequency cutoff of the sound wave spectrum, at about 0.2 Hz, the acousto-gravity wave spectrum exists. Gravity waves are excited by sub-sonic sources, including wind flow over mountains, temperature and pressure gradients, localized heating, atmospheric Rossby waves, planetary waves, tidal forcings, convection, and auroral processes. Thermospheric gravity waves often are attributed to the themospheric motions caused by the aurora via a combination of Joule heating[4] of the local thermosphere and Lorentz force[5] [*Cole*, 1971] induced plasma motion, coupled to the neutrals e.g. [*Francis*, 1975; *Hocke and Schlegel*, 1996; *Hunsucker*, 1982].

1.1.4. Solar Wind

Particles in the solar corona are excited to such a high degree that a portion of them gain sufficient velocity to escape the Sun's gravitational pull. This flow of particles outward from the sun is termed the solar wind (SW). The SW consists of electrons and positive ions (mainly protons with a small proportion of ionized helium and heavier

[4] Joule heating refers to the heating that occurs when a current flows through an object and heat is dissipated due to the resistivity of the object.

[5] The Lorentz force is the force on a charged particle of charge q caused by the surrounding electric field, $\boldsymbol{E}$, magnetic field, $\boldsymbol{B}$, and its velocity, $\mathbf{v}$ by: $\vec{F} = q\left[\vec{E} + \left(\vec{v} \times \vec{B}\right)\right]$

elements) and is therefore a charged material or plasma [*Campbell*, 2003]. The individual particles that comprise the SW are constrained to gyrate around the Sun's magnetic field lines and travel radially outward from the sun. However, the angular rotation of the solar surface where the sun's magnetic field lines are anchored causes the solar wind plasma embedded on magnetic fields to follow an Archimedes spiral pattern much like the stream of water from a rotating sprinkler. At the Earth's orbit, the direction of the spiral averages about 45° - halfway between radial and tangential - with a mean speed of approximately 400 km/s and a density varying widely from a few/cm^3 to more than 20 cm^3 about an average of 8/cm^3 [*Schulz*, 2007]. As the solar wind is a magneto-hydrodynamic fluid, it is travels along the magnetic field that is embedded at its origin in the corona, and thus defines the Interplanetary Magnetic Field (IMF) as the particle motion drags the rotating Sun's magnetic field lines into space.

Interaction between the SW and the sun's magnetic field causes the formation of a thin current sheet roughly along the ecliptic plane with the solar magnetic field lines pointing inward on one side of the sheet and outward on the other as the field lines anchored in the rotating Sun are stretched out[6]. Solar activity and the offset of the solar magnetic poles from the spin axis combined with the energetics imparted by major plasma eruptions cause this current sheet to deviate from the ecliptic plane in a pattern likened to the ruffles on a ballerina's skirt [*Campbell*, 2003]. The result of the waviness of the thin current sheet is that the Earth is alternately north or south of the current sheet, meaning that the radial component of the magnetic field seen by the Earth is alternately

[6] For a current sheet, Ampere's Law: $\nabla \times \underline{\mathbf{B}} = \underline{\mathbf{J}}$ dictates that a magnetic field with opposite directions on opposing sides of the sheet necessarily will result.

sunward or anti-sunward. Additionally, the direction of the Sun's magnetic moment switches each solar cycle, approximately 11 years.

The **B**-field component of perhaps greatest importance to the magnetosphere and ionosphere is the one that is perpendicular to the ecliptic plane, often denoted $\mathbf{B_z}$ as it corresponds to the z-direction in the commonly used Geocentric Solar Ecliptic (GSE) coordinate system, with the Earth-Sun line as the x-direction, and the y-direction is of course perpendicular to x and z. A southern IMF (negative $\mathbf{B_z}$) interconnects with the Earth's magnetic field and allows high energy SW particles to flow along these lines and into the Earth's polar atmosphere, sometimes penetrating as deep as the stratosphere [*Kelley*, 1989]. In a sense, the direction of the IMF is like a switch for solar wind penetration into the magnetosphere/ionosphere system, with a southern IMF being 'on' and a northward IMF being 'off'.

1.1.5. Magnetosphere

The Earth's *magnetosphere* is that region of space where plasma processes are dominated by the Earth's magnetic field; while outside the magnetosphere, the IMF of the solar wind dominates[7]. If there were no solar wind then the Earth's magnetic field would have an approximately dipole magnetic field due to the current systems generated in the Earth's interior. The presence of the solar wind distorts the field, 'blowing' it in toward the Earth due to the drag of the charged particles grabbing the Earth's magnetic field lines as they gyrate around them, and confining it to a windsock-shaped region. As

7 Of course the sphere of influence of the magnetic field of the Solar Wind is also finite, terminating at the heliopause, which is typically located some 110 Astronomical Units away on the upstream side of the solar system motions through our Milky Way Galaxy. Beyond the heliopause, the fields of the local interstellar medium dominate.

the SW meets the Earth's magnetic field (ignoring the bow shock caused by the supersonic nature of the SW), the Lorentz force deflects the SW electrons and ions in opposite directions, thus creating a current sheet. This current sheet compresses the magnetic field and increases the magnetic flux density on the sunward side and drags the Earth's magnetic field lines into deep space on the opposite side. The boundary thus formed between the magnetosphere and the solar wind is called the *magnetopause*; it is actually a remarkably thin region of only several kilometers thickness. The magnetopause position is dictated by the balance between the dynamic pressure of the incoming solar wind particles and the magnetic pressure of the geomagnetic field. The closest point on the magnetopause typically lies between 11-12 Earth radii in the sunward direction but can vary between 5 – 20 Earth radii. The anti-sunward part of the Earth's magnetosphere, the *magnetotail*, is more than 200 Earth radii long [*Campbell*, 2003].

1.2. Overview of the Problem

Once we had identified the COFIs and verified their existence, the next step was to determine what they are and from where they originate. A literature search quickly uncovered a similar yet transient phenomenon called Medium-Scale Traveling-Ionospheric Disturbances (MSTIDs). As their name implies, MSTIDs are traveling fluctuations in the ionosphere's density, temperature, and plasma velocity[8]. A major difference between the COFIs and MSTIDs is that MSTIDs are generally a transient 'event' phenomenon but the COFIs are apparently ubiquitous and 'steady state'. Still, as both are fluctuations in the ionosphere, it is reasonable to suspect that they maybe related

[8] A thorough review of the MSTID literature is given in Chapter 2.

or could actually be two manifestations of the same process with the COFIs being the low amplitude steady state cousins of the more intense and transient MSTID events. In fact, it is likely that some of the reported MSTIDs may have indeed been COFIs, but the limitations of the observing instruments and data processing and presentation capabilities did not allow the observers to note their ubiquitous nature. Thus the MSTID literature was taken as a starting point for the investigation.

The traditional explanation for MSTIDs is that they are in situ plasma traces of neutral atmospheric motions caused by Acoustic-Gravity-Waves (AGWs) generated in the auroral ionosphere by a combination of Joule heating and Lorentz force motion coupling e.g. [*Francis*, 1975; *Hocke and Schlegel*, 1996; *Hunsucker*, 1982]. Initially, this seemed like a good explanation for the COFIs as it fit nicely with their southwestward propagation direction as may have been observed in night-time airglow imager results (see Section 3.4) at Arecibo. An AGW hypothesis also successfully predicts the increasing vertical wavelength with height of the COFIs as seen in Figure 4.1 [*Livneh et al.*, 2007]. Although these results seemingly affirm the auroral AGW hypothesis for the COFIs, we came across several issues that cast doubt upon it.

The first such issue relates to the expected AGW dissipation based on a theoretical understanding of AGWs, both horizontally and vertically. Modern AGW theory predicts that thermospheric AGWs with the periods and wavelengths of the COFIs should dissipate within 2000 km of their source e.g. [*Vadas*, 2007]. Arecibo is at least 6000 km away from the auroral zone, however. This issue is emphasized even further by the fact that *Tsugawa et al.* [2007] saw similar MSTID structures in GPS-TEC observations over North America whose amplitude *increased* as they propagated to lower latitudes[9]. Certainly aurorally generated AGWs would not increase in amplitude as they propagate away from their source.

The AGW explanation also has difficulty explaining the vertical extent of the waves. The COFIs were observed at an altitude range spanning 100 km to over 700 km. In contrast, modern AGW theory states that AGWs with the period and vertical wavelength of the COFIs dissipate at heights less than 200 km [*Livneh et al.*, 2007; *Vadas*, 2007]. Further complicating matters is that rocket observations have shown that the plasma velocity begins to decouple from that of the neutrals at heights above ~140 km [*Sangalli et al.*, 2008]. Thus, for heights above ~200 km, the MSTID waves cannot be direct in situ plasma traces of AGWs. One scenario that saves the AGW hypothesis is that the COFIs are direct traces of AGWs below say 150 km while above this height they are the result of electrodynamic-field-aligned-forcing from the AGW-caused MSTIDs below.

Another issue with the AGW hypothesis is the lack of a consistent, coherent source that generates the requisite waves. Nevertheless, two types of AGW sources are viable candidates. The first is a tuned thermosphere/ionosphere response to the randomly timed auroral bursts at high latitudes. Using the UCL/Sheffield CTIP model, *Millward* [1994] found that such a resonance effect does exist, at least in a model, and that randomly timed auroral bursts produce thermospheric AGWs with preferred periods of roughly 45 minutes, a result that agrees with our COFI observations. The horizontal resolution of this model is too low for the COFIs however and therefore it does not

[9] When speculating on the COFIs, this and other observations of the horizontal properties of ionospheric waves have to be treated cautiously because a direct link with the COFIs is not concretely established.

account for the dissipation experienced by AGWs of the appropriate horizontal wavelengths (~200 km). The second possibility for an AGW source is that the AGWs are generated locally in the troposphere, whether orographically, by the ocean, or by weather systems.

The uncertainty surrounding the AGW hypothesis led us to look for an alternative explanation. A logical alternative to neutral atmospheric AGWs as a COFI source is that the COFIs are completely electrodynamic in nature. A possible breakthrough in this direction came when we examined Geosynchronous Operational Environmental Satellite (GOES) magnetometer data. We found that fluctuations of similar frequency to the COFIs are almost constantly present in the total magnetic field at geosynchronous altitudes (see Figure 3.15). These oscillations, likely seeded by the solar wind, can be considered as a driver for the COFIs in the ionosphere. The exact coupling mechanism(s) for these fluctuations remains unknown, but possible mechanisms are outlined in greater detail in Chapter 4. There is already some evidence of wave coupling between the magnetosphere and ionosphere in the literature e. g. *Dyrud et al.* [2008], and *Kelley et al.* [2003].

At the time of this writing, three competing theories for the nature of these waves are in play. The first, the aurorally generated AGW hypothesis, has plenty of support in the literature but is beset by several problems, namely the consistency of the source and dissipation issues. The second possibility is that the COFIS are caused by AGWs generated in the local troposphere. This hypothesis has the advantage of fitting the Arecibo observations extremely well, but here the problem is finding such a source near enough to all of the sites where the COFIs have been observed. The third, a magnetosphere / solar wind explanation shows great promise. It provides a constant source of the appropriate frequency but the exact coupling mechanism(s) between this source and the COFIs in the F-region is unknown.

1.3. List of Scientific Contributions

- Identified that vertically coherent fluctuations in electron concentration were ubiquitously present in the F-region over Arecibo, a previously unknown result.
- Found that these waves were also present over Millstone Hill Observatory.
- Developed a signal processing paradigm to extract these waves.
- Developed a rigorous testing algorithm to ensure that the ubiquitous coherent waves were not artifacts of the signal processing.
- Found that oscillations of ~45 minute period were constantly present total magnetic field at geosynchronous heights as measured GOES magnetometers.
- Searched two years barometer data from Arecibo and did not find tidal energy with a frequency similar to the COFIs.
- Developed hypotheses to explain the waves, using data from a variety of instruments and journal articles.
- Reported the above to the research community in two journal articles [*Livneh et al.*, 2007; 2009].

2. A Historical Overview of Waves in the Ionosphere

As stated in the introduction, the Coherent Omnipresent Fluctuations in the Ionosphere (COFIs) bear a strong resemblance to a similar yet usually sporadic phenomenon called Medium-Scale-Traveling Ionospheric Disturbances (MSTIDs). MSTIDs generally are thought to be plasma traces of Acoustic-Gravity Waves (AGWs) generated by auroral activity via both Joule heating and Lorentz force motions. The earliest observations of MSTIDs in the ionosphere above Arecibo were made by *Thome* [1964] using the 430 MHz incoherent scatter radar. These measurements were initiated shortly after the incoherent scatter radar was inaugurated in 1963 and three years following the seminal publication of *Hines* [1960] that addressed the theory of internal acoustic-gravity waves in the ionosphere. In 1967 a more extensive series of AGW observations was conducted at Arecibo by *Thome and Rao* [1969]. This entailed the use of the Arecibo radar along with supporting high-frequency (HF) radio wave measurements. During a three-month period extending from May through July 1967, 53 observations were performed, each of which consisted of observation periods of 3-9 hours. Traveling ionospheric disturbances (TIDs) associated with internal gravity waves were clearly identifiable in 70% of the tests. The origin of only a few of the disturbances could be attributed to geomagnetic storms or earthquakes, leaving the majority of the events to be explained in some other manner. Wave periods measured without accounting for the Doppler shift arising from the background neutral wind ranged from ~20 min in the lower thermosphere (125-200 km altitude) to 2-4 hours at higher altitudes between 200-700 km. *Thome and Rao* [1969] concluded that the TIDs were medium in scale

(~130-250 km horizontal wavelength) and that their source was probably located about 550 km from the observatory.

Incoherent scatter radar observations similar to those of *Thome* [1964] and *Thome and Rao* [1969] were conducted at Arecibo in May 1977 by *Hearn and Yeh* [1977]. This data set is more limited than that of *Thome and Rao* [1969]. Five 4-5 hour intervals showing evidence of TIDs on five different days are listed by *Hearn and Yeh* [1977]. Wave periods in the range 20-40 min were observed at altitudes between 250 and 325 km. The gravity wave model developed by *Hearn and Yeh* [1977] yielded predominant horizontal wavelengths in the range 140 to 250 km, which are similar to the HF cross spectral results of *Thome and Rao* [1969]. *Francis* [1975] reviewed the AGW observations around the globe up to that time.

Highly accurate measurements of electron concentration in the middle and lower F-region were made by *Djuth et al.* [1994] at Arecibo by applying the coded long-pulse (CLP) radar technique of *Sulzer* [1986] to plasma line echoes enhanced by daytime photoelectrons (PEPL). With this (PEPL-CLP) technique, absolute electron concentration values nominally were measured with 0.01 to 0.03% error bars at an altitude resolution of 150 m and a temporal resolution of ~2 seconds. In general, PEPL-CLP observations are considered ground truth because of their extremely low noise fluctuations and their extremely good altitude and temporal resolution, and because only a very simple background subtraction technique is needed to obtain the gravity-wave-induced concentration fluctuations. The lack of nighttime coverage is arguably the greatest shortcoming of the PEPL-CLP technique, however.

Djuth et al. [2004] noted that AGWs appear to be continuously present in the daytime Arecibo thermosphere under quiet geomagnetic conditions. They used PEPL-CLP observations made in May 1991, July 1992, July 1993, September 1994, and February 1998 to support this hypothesis. The electron concentration fluctuations were found to range nominally from 1-3%, but values as high as 8% were observed occasionally. Frequency spectra exhibited a sharp high frequency cutoff at the Brunt-Väisälä frequency, suggesting acoustic-gravity wave activity. Vertical half wavelengths were typically in the range 2–25 km between 115- and 160-km altitude. At altitudes above ~170 km, the vertical half wavelength quickly became extremely large (50–150 km).

In addition, *Djuth et al.* compares the results from the PEPL-CLP technique with those of Barker-coded power profiles (BPPs) simultaneously obtained at the centerline of the incoherent scatter spectrum. The goal was to extend the Arecibo radar coverage of gravity waves into nighttime hours with the BPPs. In general, PEPL-CLP observations are considered ground truth because of their very low noise fluctuations, extremely good altitude and temporal resolution, and because only a very simple background subtraction technique is needed to obtain the gravity wave induced concentration fluctuations. However, the limited diurnal coverage is arguably the greatest shortcoming of the PEPL-CLP technique. In the comparison study, the BPP data were lightly filtered to avoid introducing artifacts into the analysis. Sloping contours of BPP backscatter with upturning phase near 140 km altitude were found to correspond to collections of PEPL-CLP electron concentration imprints that chart the movement of electron concentration fluctuations from high altitudes (~180–200 km) to ~120 km altitude (gravity wave sets).

The time between gravity wave sets ranges from ~20–60 min. Because of statistical limitations, the BPPs do not resolve the detailed spatiotemporal structures evident in the PEPL- CLP results. Improving the filtering of the data can increase the BPP sensitivity to electron concentration fluctuations induced by TIDs however, enabling consistent observation of the waves at F2-region heights all the way up to ~800 km. It is this technique that was used to observe the COFIs at Arecibo as described in the present document.

Wave motions have been observed at a variety of altitudes and frequencies. *Philbrick* [1981] and *Philbrick et al*., [1985] observed waves throughout the mesosphere. *Philbrick et al.*, [1985] note that the mesospheric waves they observed generally had vertical wavelengths between about 3 and 10 km, a value consistent with internal gravity waves. Using a modified version of the analysis of *Hines* [1974] that includes a contribution from eddy viscosity, they calculated that these waves have horizontal wavelengths ranging from about 10 to 100 km and periods ranging from about 15 minutes to 2 hours, values similar to those of the COFIs. In the mesosphere-lower-thermosphere (MLT) region, longer period wave motions caused by a combination of long period (3-6 hours) AGWs, solar tide (8, 12, and 24-hour periods), and planetary waves (2-10 days periods) were observed over an altitude range of 75-115 km by *Cevolani et al.*, [1983] during the energy budget campaign of November to December, 1980.

In addition to Arecibo Observatory, other ISR facilities have provided evidence that waves routinely are present in the thermosphere (e.g., with the MU radar, [*Oliver et al.*, 1994] 1994; EISCAT, [*Hocke et al.*, 1996]; [*Kirchengast et al.*, 1996]; and possibly with

Millstone Hill and Sondrestrom [*Sheen and Liu*, 1988]). Referring to their MU observations, Oliver et al. remark, "it appears that the ionosphere is essentially always perturbed by gravity waves to a degree detectable with an incoherent scatter radar." In contrast to this quiet time gravity wave activity, large transient AGW events generate major ionospheric perturbations and usually are linked to a single geophysical event (e.g., geomagnetic storm, Earthquake, mesoscale convective system, etc.). Examples of such events at Arecibo are provided by *Harper* [1972] and *Nicolls et al.* [2004]. Numerous other examples may be found in the reviews by *Hocke and Schlegel* [1996], *Hunsucker* [1982], and *Francis* [1975].

In contrast to the ISR results discussed above that provide a high time and altitude resolution view of F-region waves, the superDARN (super Dual-Auroral Radar Network; http://superdarn.jhuapl.edu/) radars provide a horizontal picture of F-region wave structures over mesoscale distances as first reported by *Samson et al.* [1990]—using a predecessor to the current superDARN radars—and extended by *Bristow and Greenwald* [1995; 1996]; *Bristow et al.* [1994]; and *Bristow et al.* [1996]. *Samson et al.* [1990] report single-beam observations from Goose Bay Labrador of horizontally extended wave structures appearing in power, reflection height, and Doppler speed displayed as functions of azimuth, range, and time. These waves are reported to be most obvious under low K_p conditions, to be propagating equatorward, and to be medium scale waves characterized as having periods in the range of 27-64 minutes and horizontal wavelengths in the range of 300-500 km. They conclude that these geomagnetically quiet-time quasi-periodic waves are generated "just equatorward of the dayside flow-reversal boundary in the vicinity of the auroral electrojet at altitudes of 115 to 135 km and propagate approximately perpendicular to the boundary along azimuths ranging from 156º to 180º." They further conclude that these waves are examples of the Earth-Reflected acoustic gravity Waves (ERWs) discussed by *Francis* [1974]. Francis introduced a model for unducted MSTIDs that originate at E-region altitudes, reflect off the Earth, and, because of these origins, appear as nearly monochromatic wave packets that propagate over large horizontal distances with little attenuation and show a linear increase in period and wavelength with distance from the source. Francis further notes, "consideration should be given to the auroral electrojet as an important source of medium-scale TIDs…" Modeling studies reported by *Vadas* [2007] however indicate that directly propagating, i.e., not Earth-reflected, AGWs originating at ground level or at 120 km altitude will propagate a horizontal distance of only 1000-2000 km before dissipating in the thermosphere above ~200 km altitude due to kinematic viscosity and thermal diffusion.

Events in the troposphere have been shown to generate AGWs that in turn produce MSTIDs [*Lastovicka,* 2006]. In particular, the passage of tropospheric storms has been shown to induce an increase in detectable ionospheric wave activity. [*Boska and Sauli*, 2001] and [*Sauli*, 2001] showed that the passage of a cold front through the troposphere caused a significant increase in ionospheric AGW activity in the 50-120 minute period range. Using a dense array of Global Positioning System (GPS) receivers in Japan *Lognonne et al.* [2006b] and *Lognonne et al.* [2006a] demonstrated that seismic activity as far away as Peru could be detected easily as fluctuations in the ionosphere's total electron content.

In recent years, several authors have suggested that the waves that they observed in the mid-latitude ionosphere are not imprints of acoustic gravity waves but instead are ionospheric manifestations of oscillations observed in the magnetosphere and the solar wind. *Dyrud et al.* [2008] reported observing the effects of solar wind oscillations in the ionosphere over Arecibo. They observed 0.1% variations at a frequency of 1.7 mHz (~10 minute period) in the Arecibo plasma frequency at the F-region peak that they link to the commonly observed solar wind fluctuations of similar frequency e.g. *Kepko and Spence* [2003]. Further evidence of solar wind effects on the ionosphere was reported by *Kelley et al.* [2003] and *Huang et al.* [2007] who found that oscillations in the Interplanetary-Electric-Field (IEF) measured by the Advanced Composition Explorer (ACE) satellite caused morphologically similar variations in the electric field of the equatorial ionosphere. The possibility of the solar wind and magnetospheric origin of these COFIs is addressed more thoroughly in Chapter 4.

Radar is not the only instrument with which MSTIDs have been observed. An informative set of results come from *Tsugawa et al.* [2007], who used a North-America-wide network of GPS receivers to get a wide look at Total Electron Concentration (TEC) through the ionosphere. The TEC fluctuations that they report exhibit a consistency that is evocative of the COFIs. They report two interesting findings. First, they note that the waves differ between the daytime and nighttime. During the day, the waves are seen to travel to the southeast and have wavelengths of 200-500 km. At night, the waves change direction, and now travel towards the southwest with a longer horizontal wavelength of 300-1500 km. The propagation speed of the waves during the day was recorded as 100-150 m/s, but at night there were some faster waves on occasion, with the speeds now ranging from 100 to 200 m/s. Second, they note that for their coverage range of 30-65°

N magnetic latitude, the observed MSTID amplitude increases as the waves propagate toward lower latitudes.

Nighttime MSTIDs also have been observed extensively in airglow imager (see Section 3.4) data. *Seker et al.* [2008] present airglow images from the Penn State All-Sky Imager (PSASI) at Arecibo observatory that coincide with the Arecibo incoherent-scatter-radar (ISR) observations from 22-24 March shown here in Figure 1.2. They show that traveling airglow depletions move towards the southwest at speeds ranging from 35 to 100 m/s and have horizontal wavelengths of 100 to 300 km. *Garcia et al.* [2000] also observed MSTIDs in airglow images from Arecibo and give speeds of 50 to 170 m/s and horizontal wavelengths of 50 to 500 km. Similar MSTIDs often have been observed in airglow imagers over Japan e.g. [*Taylor et al.*, 1998], [*Saito et al.*, 2001], [*Shiokawa et al.*, 2002; *Shiokawa et al.*, 2006], and over Japan and at its geomagnetic conjugate point in Australia [*Otsuka et al.*, 2004]. *Shiokawa et al.* [2002] present a combination of TEC and airglow imager observations to demonstrate that MSTIDs tend to weaken at a substantial distance before they reach the magnetic equator and vanish below about 18° magnetic latitude.

3. Observations and Signal Processing

This chapter contains the actual observations of the Coherent Omnipresent Fluctuations in the Ionosphere (COFIs) and the signal processing methods that were used. Section 3.1 is a step-by-step guide through the signal processing applied to the ISR data to highlight the COFIs and shows the data sets at varying degrees of processing. As the COFIs are a newly identified phenomenon, it is important to substantiate their existence by ensuring that they are not artifacts of the signal processing. To that end, Section 3.2 gives a rigorous defense via various validating tests of the signal processing procedure outlined in Section 3.1. In Section 3.3, the processed results from the various ISRs are presented and discussed. Section 3.4 describes a multi-instrument search for clues to the nature of the COFIs and includes microbarograph and airglow observations from Arecibo along with satellite observations from the GOES and ACE satellites.

3.1. COFIs revealed: a step-by-step tour of the signal processing

In this section, all of the signal processing steps are outlined carefully in order to assure the reader that the wave results seen in Figures 3.1-3.3 are not in any way an artifact of the signal processing. As the COFIs were originally discovered in Arecibo power profile observations from 22-24 March 2004 and 5-7 June 2005 [*Livneh et al.,* 2007], these data sets are taken as an example to demonstrate the procedure. All ISR data sets consisted of a rectangular array of data, with time varying along one dimension and altitude varying along the other.

Before delving further, the filtering algorithms used are described. With the exception of neighbor averaging, all of the filtering operations described in this Section were done in the manner described below. First, note that the filtering was done independently for each column (time) and altitude (row), depending on the dimension (time or altitude) along which the data were being filtered. That is, for filtering in the time (horizontal) direction, the filtering was done independently for each constant-altitude (horizontal) strip, while filtering in the altitude (vertical) direction was done independently for each constant-time (vertical) strip. Filters were implemented in the frequency domain using a Hamming Window Fourier Series method. The Hamming window was chosen because it provided a very reasonable frequency response with relatively few coefficients, a characteristic that is desirable for analyzing data sets of limited length. The following steps were taken. First, a Fast-Fourier-Transform (FFT) was performed on a mean-removed data series corresponding to each constant altitude (or time) strip, depending on the direction of filtering. The complex spectrum of the strip was multiplied by the complex Fourier series of a finite impulse response (FIR) filter based on a Hamming window. Then the result was inverse-Fourier-transformed into the time (or altitude) domain, and its real part was taken as the filtered output.

Several stages of signal processing were performed on the raw—pulse-by-pulse level—data in order to examine these low-level fluctuations of the ISR signal about the mean. First, the raw voltage data was pulse-by-pulse processed to remove interference and meteors as outlined in *Wen et al.* [2006]. This data level was then averaged over 1000 inter-pulse-periods (IPPs) to give a new interval of 10 seconds between data points. Next, using the noise and noise plus calibration source regions of the averaged noise profiles, the noise baseline was subtracted and the profile was converted to signal temperature, which is proportional to electron concentration at each range, as described by *Mathews* [1986]. Note that the signal temperature rather than the electron concentration plots of the Arecibo data are have been shown here to avoid non-linear processing.

Some minor smoothing was then performed to mitigate any high-frequency noise that might appear in the final result. This process consisted of three parts. First, each pixel was averaged with its nearest neighbors by summing the pixel itself with the 4 nearest-neighbor pixels and then dividing this result by 5. Note that the pixel was averaged with its *original* nearest neighbors, not its already averaged neighbors. Then, the data were low-pass filtered, first in the altitude direction, eliminating changes of less than 3 km in scale and then in the time direction, eliminating variations with periods of less than two minutes. These steps yielded the results shown in Figure 3.1. The geomagnetic index (K_p) has been included in several of the figures in this document soley to show whether the corresponding radar data was taken from a quiet or active geomagnetic period.

Now that the low-pass filtering (smoothing) operations that—along with interference/meteor removal—yielded the Figure 3.1 results were completed, the **most significant** step of the signal processing was ready to be performed. This was high-pass filtering in the time (horizontal) direction that highlights the wave-like features by attenuating the features due to the diurnal variations of the underlying ionosphere. This produced the results seen in Figure 3.2. The high-pass filtering has stop- and pass-band edge periods of 2- and 1-hours, respectively. The rejected (stop-band) frequencies are attenuated by a factor of at least 1000, according to the filter specifications. For comparison, the spectrum of a strip of the original data compared with the spectrum of the processed data is shown in Figure 3.3.

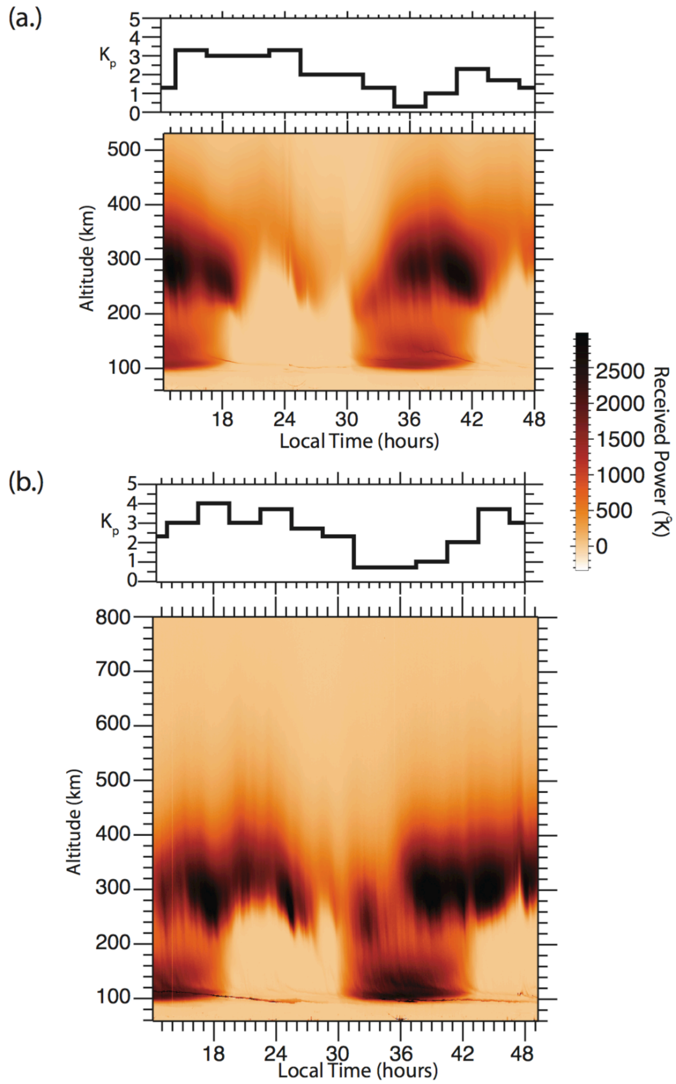

Figure 3.1. The Arecibo ISR datasets shown as Range-Time-Intensity (RTI with intensity expressed in Kelvins on the sampled bandwidth) images after pulse-by-pulse (10 msec InterPulse Period—IPP) cleaning (interference and meteor removal), noise subtraction, averaging over 10 seconds, and conversion to signal power [*Mathews*, 1986]. The waves can be seen in these images as the near vertical parallel stripes faintly visible in both images. The panel (a) results span 1200 Atlantic Standard Time (AST) 22 March 2004 through 2300 AST 23 March 23 2004—a total of 35 hours. Each signal temperature profile contains 1575 samples corresponding to 59-530 km altitude with 0.3 km resolution (0.6 km feature resolution). Panel (b) is similar to (a) but begins at 1300 AST 5 June 2005 and ends at 0100 on 7 June 2005. For this dataset, each power profile contains 2490 samples corresponding to heights spanning 59-800 km with 0.3 km resolution. The geomagnetic activity (K_p) values with observation periods indicated are shown at the top of each image.

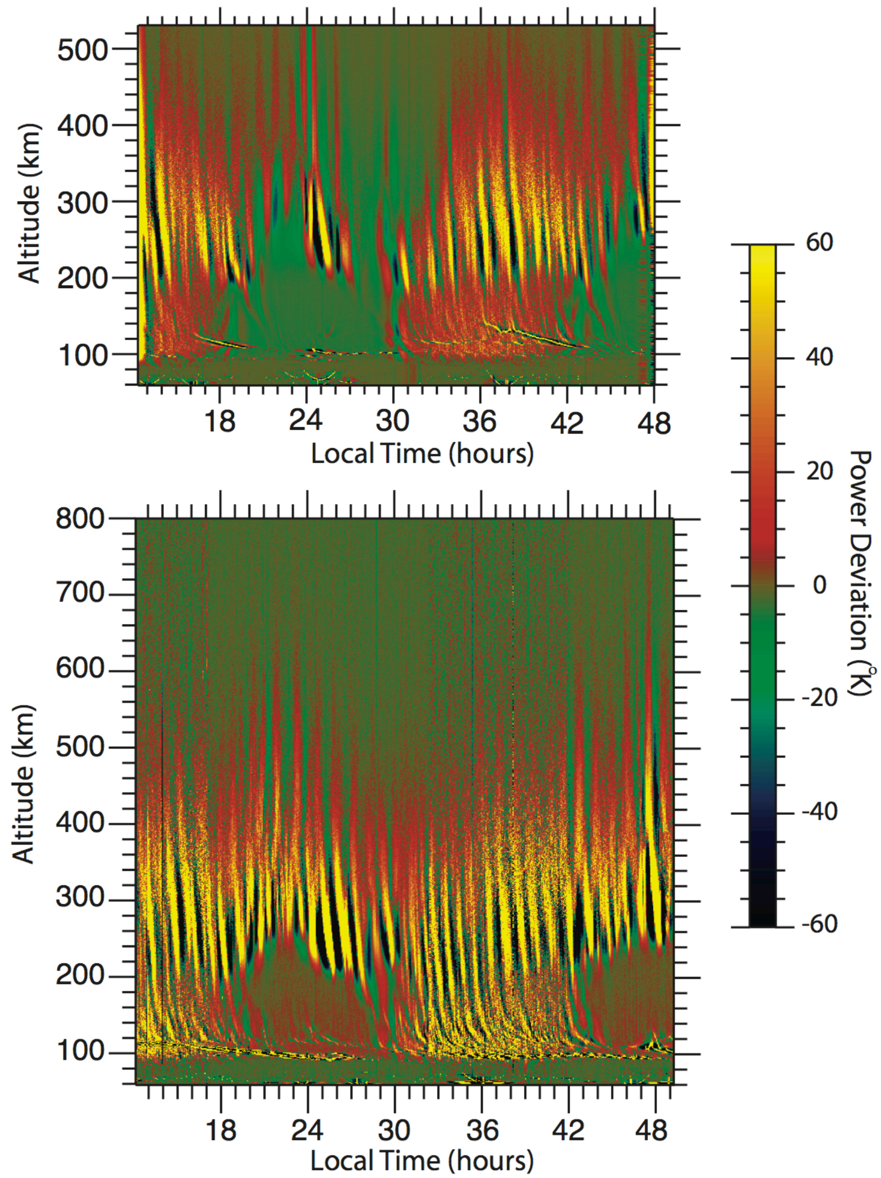

Figure 3.2. RTI images of the high-pass filtered results for the 22-24 March 2004 and 5-6 June data sets whose originals were seen in Figure 3.1. These results clearly show the waves (near vertical parallel stripes) with quasi-periods of ~1 hour that were seen more faintly in Figure 3.1. These results are given in terms of signal power expressed in °K and are not range-squared corrected [*Mathews*, 1984; *Mathews et al.*, 1982] and converted to electron concentration so that the waves seen here are subject only to linear processing. Notice that the waves appear very clearly here where one can view their vertical extent. Contrast this view with the less coherent appearance of the waves as seen in a constant altitude strip (Figure 3.15) taken from the processed data near the peak of the ionosphere (~300 km). The vertical coherence of the waves shown here is further proof of their validity because the processing is done independently at each altitude.

3.2. Validation of the Signal Processing Procedure

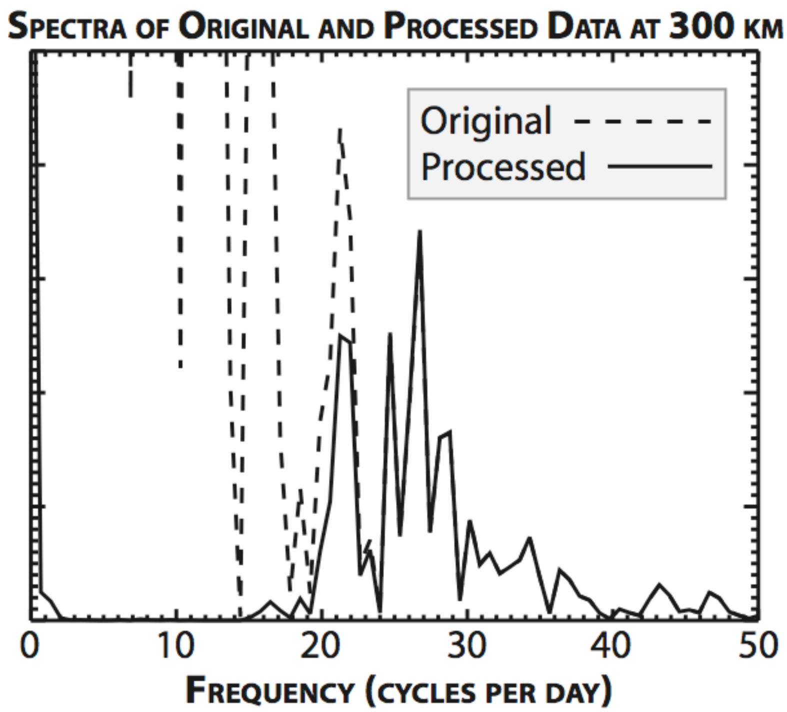

Figure 3.3. A comparison of the FFTs of the original (dashed line) with the high-passed (solid line) data from June 2005 at an altitude of 300 km. Notice that the filtering process does not introduce any artificial frequency components into the result.

With any signal processing comes the risk that the features present in the processed data are due to the processing itself and do not exist in the original data. Three tests, outlined next, were performed on the net processing algorithm used for wave extraction. The first verifies that the waves are not due to virtual band-pass filtering inherent in the power law spectrum of the net distribution of 'wave' processes that constitute the spectrum. The second test examines whether waves that were present in the data were extracted correctly. Finally, the third test determines if the wave features could be due to the well known ‘ringing’ of filters (Gibbs Phenomenon). The following subsections present the results from these tests.

3.2.1. Test on Noise with Spectral Content Identical to the Data

A concern whenever data are band-pass filtered is that the waves that are seen in the output are the result of restricting bandwidth and thus enhancing apparent coherence or wave-like appearance of noise or otherwise incoherent features within the original data. In these observations, as with many geophysical quantities, noise power at the higher frequencies is naturally ‘cut-off’ as f^{-n} owing to the natural power law decrease in spectral content with frequency—e.g., see *Canavero and Einaudi* [1987]. For extraction of the wave-like features seen in Figure 3.1, high-pass filtering is performed, resulting in a power spectral peak near the filter cutoff. That is, the spectrum has effectively been band-passed, creating the risk of seeing apparent but false wave content. To this end, the test discussed next was devised.

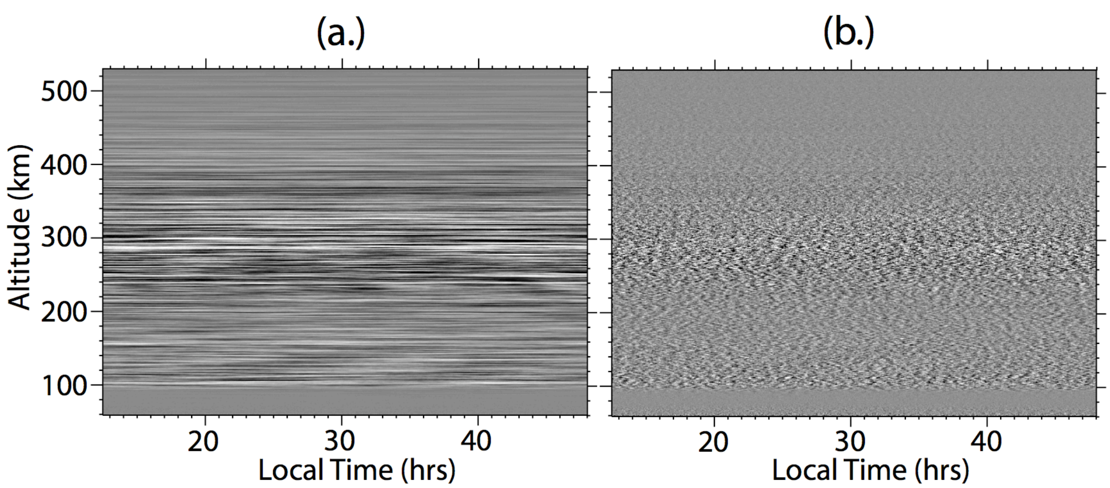

Figure 3.4. Before (a.) and after (b.) images of noise with an identical power spectrum to the March 2004 data. Coherent wave features are not present in the processed result, implying that the waves seen in the actual data are real, and not due to virtual band-pass filtering.

Noise with a spectrum identical in magnitude to that of the signal temperatures from 22 March 2004 was created via the following steps. First, the Fast-Fourier Transform (FFT) of the signal temperatures was computed and its absolute value was taken. This spectrum was then multiplied by an array of random values all with unity magnitude and uniformly distributed phase. That is, the approach yielded a spectrum with the same frequency distribution as that of the March data but with a randomly distributed phase. The inverse FFT of this spectrum resulted in a noise "signal" in the time domain, shown in Figure 3.4a, with a power spectrum identical to the March data but with randomly distributed phase. This noise data were then passed through the entire filtering process, yielding the plot seen in Figure 3.4b. If the waves were truly due to effectively band-pass filtering the data, then Figure 3.4b would show the near vertical stripes clearly seen in Figure 3.2a.

Neither altitude nor time coherent wave-like features are present in the processed result because the phases of constant altitude strips in the noise do not align with each other as they do in the actual data. Thus, although it is difficult to pinpoint the waves themselves on a plot of the spectrum of the raw data (see Figure 3.3), clearly vertically-coherent structures do exist in the observations, as seen in Figure 3.2. Moreover, these structures are not due to limiting the bandwidth of the plotted data.

3.2.2. Proper Extraction of Wave Features

The next test of the signal processing system determines the effectiveness with which model waves inserted on top of a background 'F-layer' with noise can be extracted successfully. A 28-hour F-region signal temperature data set was roughly simulated by placing two Gaussian 'bells' side by side in the time direction and then multiplying them by another Gaussian bell in the altitude direction. Although this model is obviously far from an accurate depiction of the actual ionosphere, it is certainly suitable for the purpose of verifying the efficacy of the signal processing because the dynamic range over which the "wave signal" is embedded in the background "ionosphere" signal approximates the signal environment of the Arecibo data. Gaussian-distributed noise was also added to model the noise seen in the ISR data. As in the actual data, the time and altitude resolution were modeled as 10 seconds and 0.3 km, respectively. To this, waves of period 1-hour were superimposed, yielding the image seen in Figure 3.5a. After processing, the result (Fig 3.5b) is seen to contain simply the waves themselves with a very slight modulation because of the original background 'F-region' signal that was attenuated by the low-pass filter processing. The effects of the processing on a time series taken from the heart of the model ionosphere are seen in Figure 3.5c, which shows a constant altitude strip before and after the processing.

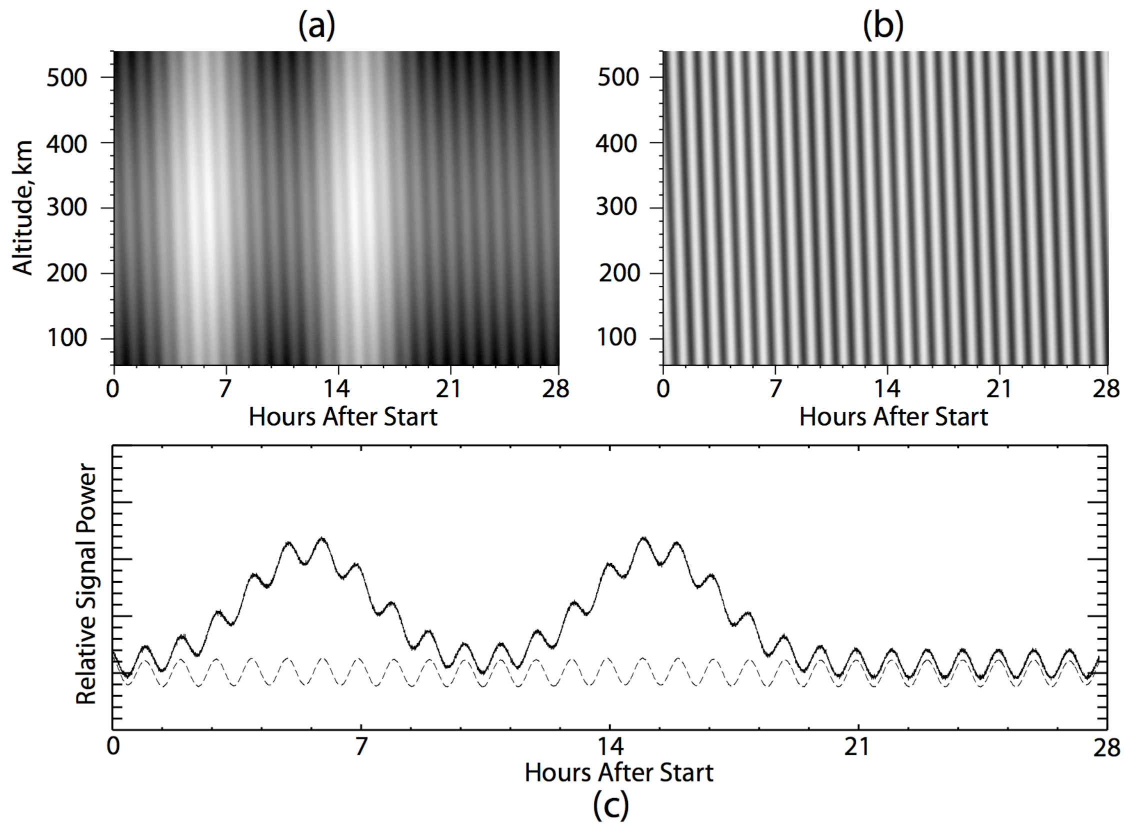

Figure 3.5. Test for correct extraction of the waves as described in the text. Panel (a.) shows the original test data created—it includes an 'F-region', noise, and waves. Panel (b.) shows the result of the same signal processing applied to convert the Figure 3.1 to Figure 3.2 results—the waves have been extracted successfully without undue distortion from the filtering process. Panel (c.) shows a slice through both images at 300 km. Here, the solid line gives the original data and the dashed line shows the processed result.

3.2.3. Spike Test for Gibbs Phenomenon

The third and final test of the processing routine verifies that the waves of Figure 3.2 are not simply a result of 'ringing' in the filter impulse response e.g. [*Mathews et al.*, 1985], which is known as the Gibbs Phenomenon. To this end, the background 'F-layer' discussed relative to Figure 3.5 was modified to include a 'spike' as seen in Figure 3.6. After applying the same signal processing approach as before, the spike remained, along with very small side lobes—these side lobes are not sufficient to cause the appearance of waves.

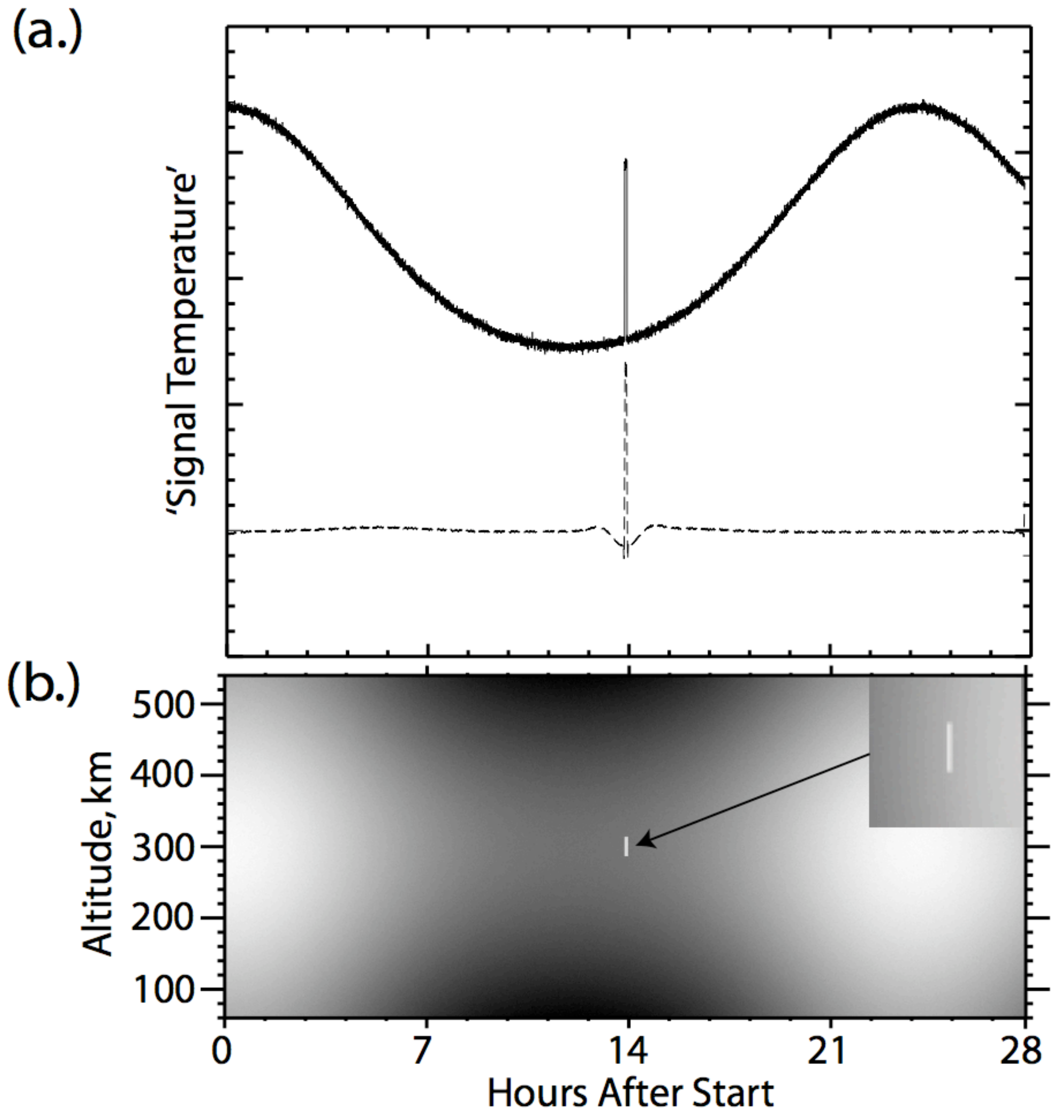

Figure 3.6. A 'spike' is added to the 'F-layer' model in Figure 3.5 without waves to test for 'ringing' of the filtering process. Panel (a.) shows a slice through the spike—shown in panel (b.) at 300 km—in the test data. The solid and dashed lines in panel (a.) show the slice before and after processing, respectively. Note that the ringing is much too small in amplitude and duration to create the quasi-periodic wave-like structure found in the actual data.

3.2.4. Wave Extraction via Non-Ringing Discrete Prolate Spheroidal Filter

As a further check to ensure that the waves shown in Figure 3.2 are real and not simply filter artifacts, the images were processed using a non-ringing Discrete Prolate Spheroid (DPS) filter. For a detailed description of the DPS filter and its properties, please see [*Mathews et al.*, 1985]. The images obtained using the DPS technique are shown in Figure 3.7.

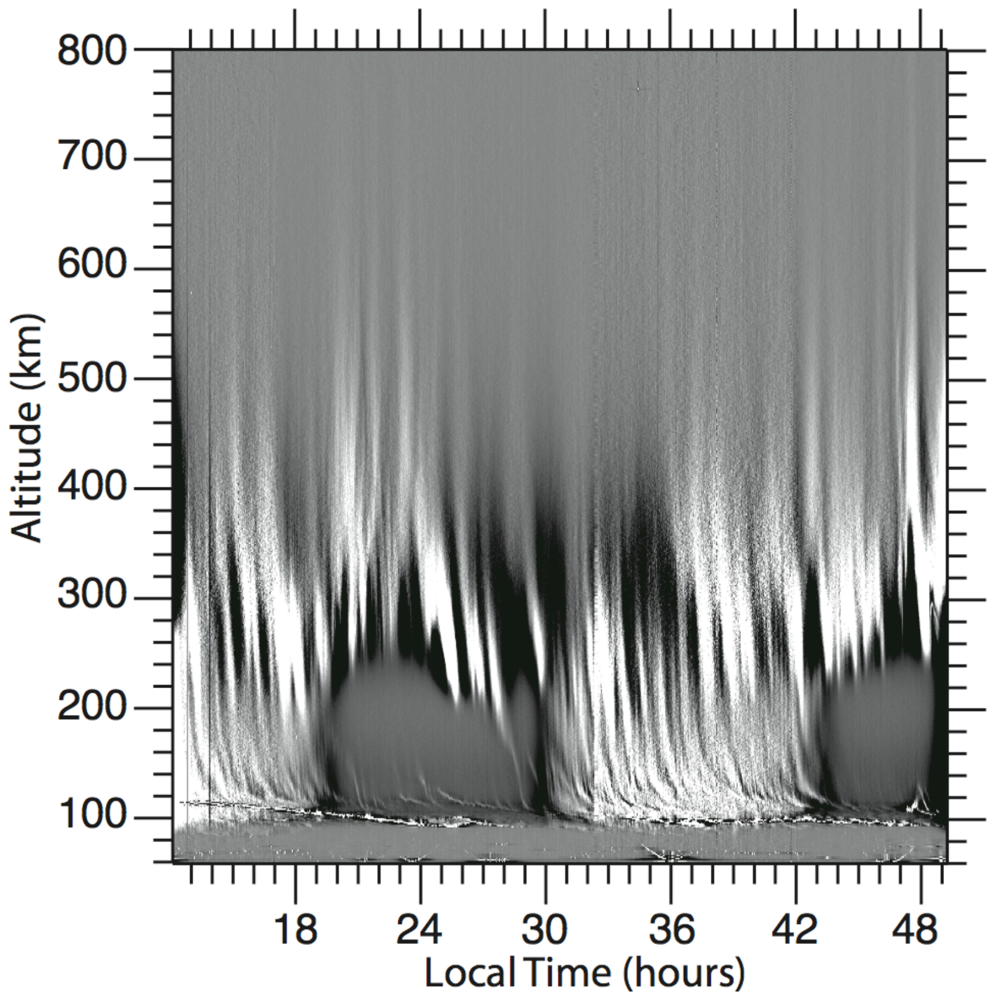

Figure 3.7. Waves extracted from the 5-7 June 2005 observations using a Discrete Prolate Spheroidal (DPS) filter instead of a Hamming Window. Although the DPS filter is non-ringing, it also has an extended transition from pass- to stop-band causing wave features to washout. For this reason, the Hamming filter was used to find the detailed results shown in Figure 3.2.

The results obtained using the DPS filter clearly show the wave-like features seen in Figure 3.2 though not as clearly as those obtained using the Hamming window approach, because the DPS technique sacrifices more ideal frequency response with a well-defined cutoff frequency in favor of eliminating *all* ringing. DPS-based filters do not approximate the ideal low-pass filter frequency response, but instead approximate a Gaussian response in both the time and frequency domains. That is, they have a steadily decreasing response as the frequency is increased. Thus, there is not a sharp distinction between pass- and stop-bands, simply a smooth roll-off as shown in Figure 3.3 of [*Mathews et al.*, 1985]. Therefore, DPS filters cannot reject and accept the desired frequency ranges as readily as filters based on a more ideal frequency response such as those based on Hamming Windows. Nevertheless, application of the non-ringing DPS filter to the Figure 3.1 data produces strong evidence of the Figure 3.2 wave structure as seen in Figure 3.7.

3.3. COFIs in ISR observations

Section 3.1 gives a step-by-step tour of the signal processing methods used on the ISR data. Section 3.2 presents a rigorous defense of the processing methods presented in Section 3.1 and re-affirms the validity of the results and the existence of the waves. In this Section, observations of the waves in other Arecibo Observatory (18.3° North, 66.8° West) data sets and also in data sets obtained from other ISRs, namely those at Millstone Hill, Massachusetts (42.6° N, 71.5° W) and at Poker Flat, Alaska (65.1° N, 147.4° W) are presented.

3.3.1. Arecibo Radio Observatory, Puerto Rico

The COFIs were originally discovered in two Arecibo ISR (18.3° North, 66.8° West) data sets from 22-23 March 2004 and 5-6 June 2005 [*Livneh et al.*, 2007]. Please refer to Section 3.1 for images of these data sets because those figures are not reproduced in this Section. These observation sets each contained roughly 35 hours of power profiles taken using a 10 ms Inter-Pulse-Period (IPP) and the standard 13-baud, 4 μsec/baud, Barker code technique, yielding—using 2 μsec sampling—600 meter altitude resolution. The data sets after cleaning (interference/meteor removal per [*Wen et al.*, 2006; 2007]), downsampling, and conversion to signal power (expressed in Kelvins) are shown in Figure 3.1 as range-time-intensity (RTI with intensity in Kelvins) images of the ionosphere. *Mathews* [1986] discusses the Barker code technique as well as the conversion of relative incoherent scatter total - signal plus noise - power to signal power expressed in Kelvins in the sampled bandwidth.

Quasi-periodic wave structures are pervasive through both of the Figure 3.1 processed results without filtering at any level. Figure 3.2 shows RTI plots of the waves "extracted" from the Figure 3.1 data sets using the high-pass filtering techniques described in Section 3.2. Figures 3.8 and 3.9 are similarly processed results from 21-25 September 2005 and 17-21 November 2005, respectively. Waves are seen throughout all of the data periods shown, albeit more clearly in regions of higher rather than lower ionization. At all times and in all data sets, the waves are clearly visible for altitudes between ~200 and ~450 km. All of the data sets also clearly contain waves in the daytime F1 layer (~120-200 km). For the three data sets whose altitude range is capped at around 530 kilometers (March 2004, September 2005, November 2005), the COFIs often appear to extend beyond the upper altitude edge of the data. In the June 2005 results where the altitude coverage is greater, the waves are even seen to extend to the top of this image at times, an altitude of 800 km. There is no reason to doubt that this would also be the case in the other observations if they too had extended up to the same heights. Traces of the waves are also seen in the nighttime F1-region wherever and whenever there is sufficient plasma.

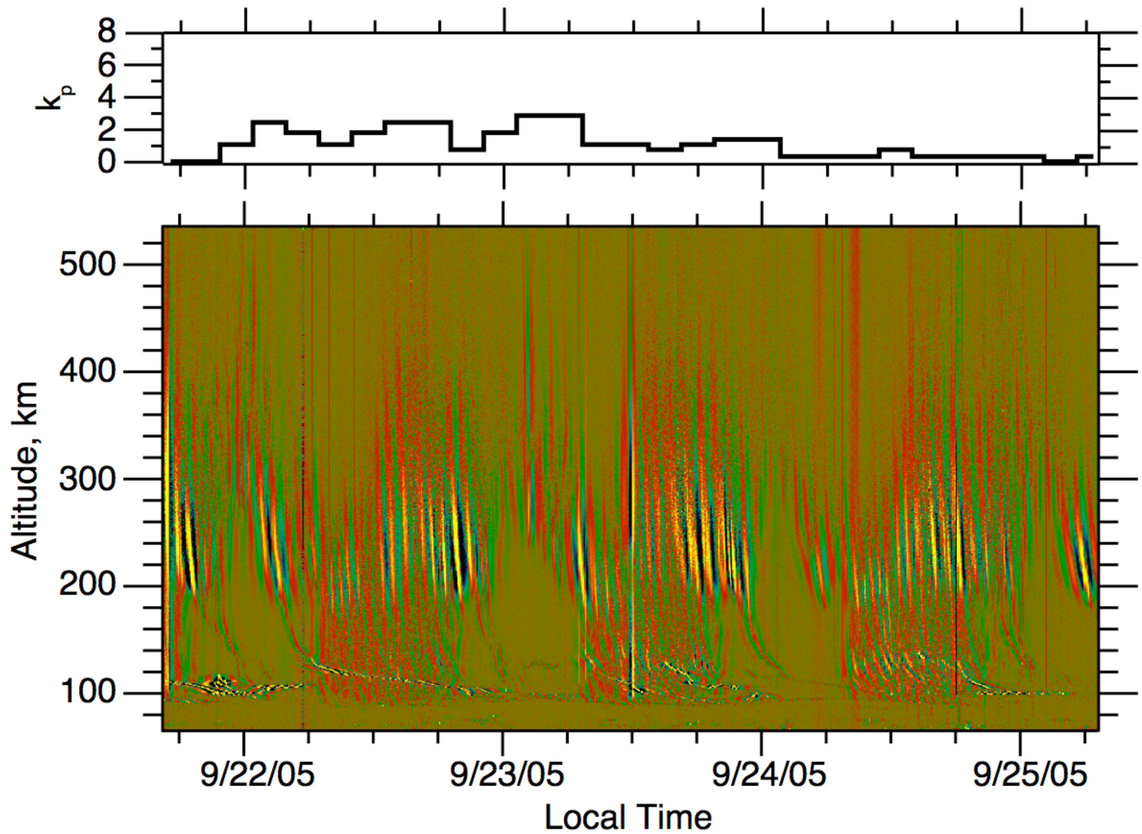

Figure 3.8. High-pass filtered power profile data for 21-25 September 2005 from Arecibo Observatory with the geomagnetic index, Kp shown above. The COFIs are clearly visible as the near vertical 'stripes' present throughout much of the plot. These stripes (COFIs) appear at all times and at all altitudes where the background ionosphere is sufficiently ionized to provide adequate signal-to-noise ratio for the ISR. Notice the plot shows that the COFIs become more vertical with increasing height, a property characteristic of thermospheric acoustic gravity waves.

Suggestions of the unambiguous wave imprints - near vertical stripes - seen in the high-pass filter processed plots of Figure 3.2 actually can be seen in the **unfiltered** plots of Figure 3.1. The effect of filtering is simply to highlight these wave structures by attenuating the larger-scale features—largely due to the diurnal electron concentration variations—present in the Figure 3.1 results. As an example, the positive effect of filtering is particularly evident in the June F1-region results near 30 hrs where unfiltered Figure 3.1b results are unclear although the Figure 3.2b results show considerable detail at that time and altitude. Figures 3.1 and 3.2 utilize signal power (in Kelvins) so that all processing is linear, thereby avoiding distortion across the altitude dimension.

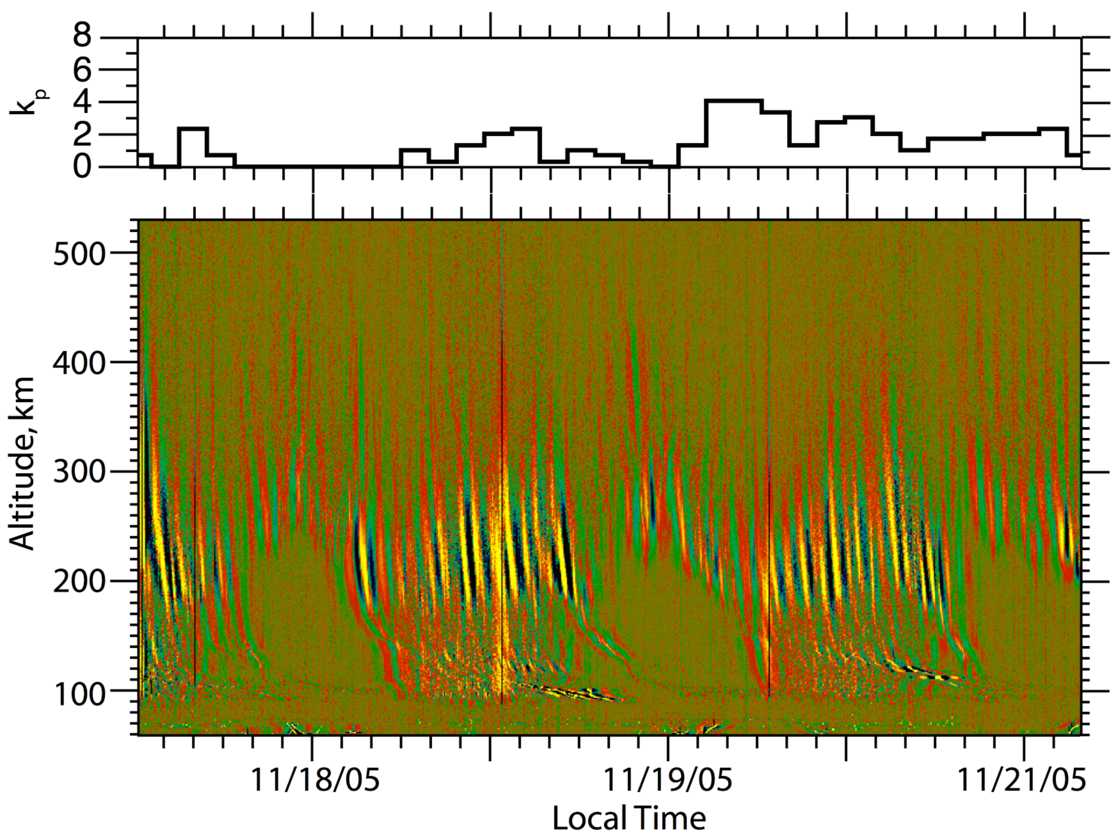

Figure 3.9. Another processed power profile data set from Arecibo, this time from 17-21 November 2005. Once again, the COFIs are pervasive throughout the observation period.

Another instructive way to look at the COFIs is to determine how much they cause the ionosphere's electron concentration to fluctuate relative to its background level. This is achieved in Figure 3.10 by plotting the strength of the COFIs in terms of percentage deviation of electron concentration with respect to the background ionosphere. The image in Figure 3.10 is the result of dividing the high-passed wave result of Figure 3.2 by the 'original' ionosphere plot of Figure 3.1 with the following modifications. To get the same signal level from the same electron concentration at different ranges in principle the data should be range-square corrected at all altitudes *Mathews* [1986] because the incoherent scatter signal power level falls off as the square of the range. Since the normalized amplitude of the waves expressed in electron concentration is of interest, the Figure 3.2 results are range-squared corrected - after filtering - and then divided by the range-squared corrected version of the background ionosphere represented in the low-pass filtered version of the Figure 3.1 results yielding Figure 3.10. Because the background ionosphere is very weak at high altitudes and at times in the nighttime F1-region, the range over which this normalization processing succeeds is limited to regions of sufficient ionization. This normalization procedure reveals the waves to look even more coherent vertically than before—they now appear much more as constant amplitude, parallel stripes with shorter vertical wavelength, or more tilting, at the lower altitudes and much larger vertical wavelength at the higher altitudes.

In an attempt to quantify the impact of the COFIs on the ionosphere, the typical percent deviation caused by the waves was calculated. For each observation period, the standard deviation of the relative power was taken over all times and for the altitudes ranging between 298 and 358 km. This altitude range was chosen for its high signal-to-noise ratio because it is near the F2-peak. The averaged standard deviations were found to be 0.039 and 0.038, 0.043, and 0.048 for the March 2004 and the June, September, and November 2005 results, respectively. If the waves are assumed to be approximately sinusoidal, then this gives respective average wave amplitudes of 0.056, 0.053, 0.061, and 0.066 relative to the background ionosphere. The amplitude similarity between the data sets suggests that the same source and source strength are responsible for the waves in all observation periods.

The vertical wavelength of the COFIs was measured by drawing a vertical line through Figure 3.10 and finding the two local maxima nearest to a given altitude. The distance between these two maxima is taken as the vertical wavelength at that altitude. As seen in Figure 3.10, the waves have a vertical wavelength of approximately 25 km at 110 km (daytime) increasing to over 200 km above 300 km altitude, with the distinct downward phase progression as time increases that is characteristic of AGWs. This vertical wavelength is similar to the value found by *Oliver et al.* [1997] using the Japanese Middle and Upper atmosphere (MU) radar and Figure 13 of [*Djuth et al.*, 1997] using the Arecibo radar.

Throughout all of the processed plots from Arecibo, the waves display a ‘hockey stick’ shape. That is, the ‘stripes’ become more vertical with increasing altitude. This characteristic implies that their vertical wavelength increases with height, evocative of acoustic gravity waves at these heights due to the upward temperature gradient in the thermosphere. Neutral and plasma motions decouple above about 200 kilometers e.g. [*Sangalli et al.*, 2008] however, and so the direct local effect of such AGWs will be severely curtailed. Also interesting is that there are no shorter-period (<35 minute) oscillations seen in the upper F-region, above say 350 km, while the lower F-region (below 200 km) is rife with these relatively higher frequency waves. A full examination of these topics is given in Chapter 4.

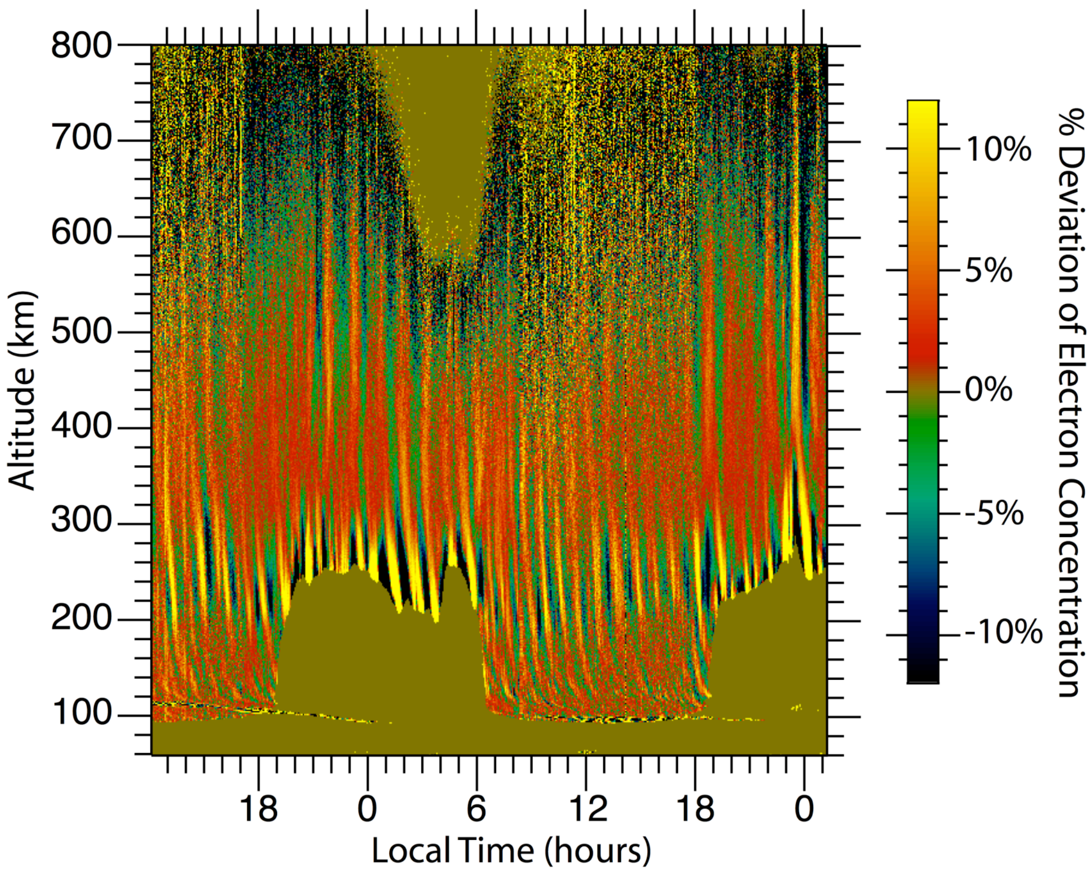

Figure 3.10. The filtered June 2005 result shown in Figure 3.2b but range-squared corrected and converted to the percentage deviation in electron concentration by normalizing it with the background (unfiltered) ionosphere results from Figure 3.1b. The waves are seen to have a deviation of around ±0.075 (7.5%), peaking near ±0.12 (12%) in the nighttime F-region base. However, the largest apparent deviations are likely due to the weakness of the background ionization, caused by division by a near zero denominator, and thus are suspect. Note that in this data, range-squared correction shows the waves to be of approximately constant amplitude. Portions of the nighttime F1-region and a region above 600 km have low SNR and were set to zero because percentage deviation could not be calculated.

Taken together, the four Arecibo data sets presented here constitute more than nine days of observations and span two years and three seasons. The COFIs are seen ubiquitously at all times and at all altitudes throughout these four data sets, implying that they are likely to be always present. Regretfully, all of these observations were taken during geomagnetically quiet times. Luckily, observations from more geomagnetically active periods were obtained from the ISR at Millstone Hill.

3.3.2. Millstone Hill Observatory, Massachusetts

One month of electron concentration (N_e) data was recorded at Millstone Hill, Massachusetts (42.6° North, 71.5° West) from October 4 to November 4, 2002 with a 68-meter zenith antenna using interleaved single pulses and alternation-coded pulses [*Zhang et al.*, 2005]. Despite the lower signal-to-noise ratio and erratic sampling period of this observation set, the COFIs are still visible throughout the plots. Two 2-day segments of the month-long data set are shown in Figure 3.11, one during a period of low geomagnetic activity, and hence low geomagnetic activity index, *Kp*, and one during high geomagnetic index. The COFIs are seen in both plots, regardless of geomagnetic activity, albeit with somewhat greater intensity during elevated *Kp* (Figure 3.11b) than during the quieter period (Figure 3.11a). The clear presence of these waves at both Millstone and Arecibo suggests a wide geographical extent for these waves and undermines the hypothesis that these are locally generated AGWs. Although the data quality makes it difficult to state with certainty, the COFIs appear to have a longer vertical wavelength (stripes are more vertical) than at Arecibo. This change may be due to the much higher geomagnetic dip angle at Millstone.

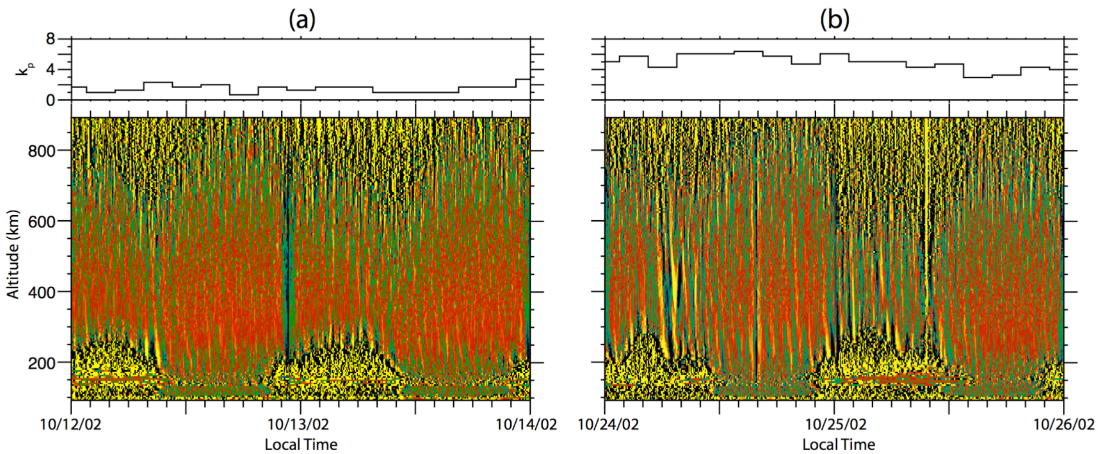

Figure 3.11. Two 2-day periods of processed electron concentration data from Millstone Hill Observatory, Massachusetts, with the concurrent geomagnetic index *Kp* displayed above. As in the Arecibo results, the COFIs are seen throughout these observations and throughout the remainder of the observations for the entire month. These two plots were selected for their levels of geomagnetic activity. Figure 3.11a (left) presents results from a relatively geomagnetically quiet (low *Kp*) period and Figure 3.11b (right) was taken during a more geomagnetically active period (elevated *Kp*). Notice that although the COFIs are prevalent in both plots, they are even stronger during the period of higher geomagnetic activity (Figure 3.11 b).

3.3.3. Poker Flat Incoherent Scatter Radar, Alaska

The F-layer is created by photoionization and is therefore contingent on the direct impact of sunlight on the thermosphere. At the high latitude where the Poker Flat Incoherent Scatter Radar (PFISR) is located (65.1° North, 147.4° West), the presence of the F-region is highly seasonally dependent, because the area receives nearly constant sunlight during the summer but is nearly continuously dark during the winter months. Because we are searching for a continuous F-region wave phenomenon, and because the winter F-layer is only present for brief periods daily we must examine data from near the summer solstice. Even in the summer, the F2 layer that is prominent at midlatitudes is very weak at these latitudes and we generally see only the F1-layer, which of course only exists in the daytime. Luckily, during the summer at high latitudes, the ‘daytime’ is actually rather extended. With this in mind, we obtained N_e data from near the summer solstice (June 29 to July 3, 2007) and processed it in the same manner as the Arecibo and Millstone data sets to search for the COFIs (Figure 3.12). These observations were taken looking parallel to the local geomagnetic field lines to eliminate the possible effect of looking across field lines, as is discussed below.

These observations show *sporadic* - not *consistent* - evidence of the COFIs. The data quality is poor compared with the Arecibo and Millstone Hill observations, and thus it cannot be concluded that the waves are or are not *always* present here. Still, the more sporadic nature of these observations *may suggest* that the COFIs are limited to mid-latitudes or even to the east coast of North America. The data quality is too poor to make conclusions about the existence – or lack thereof - of the COFIs over Poker Flat however, and as such no implications about the geographical variation of the COFIs can be made. Please see Chapter 4 for a full analysis of these results.

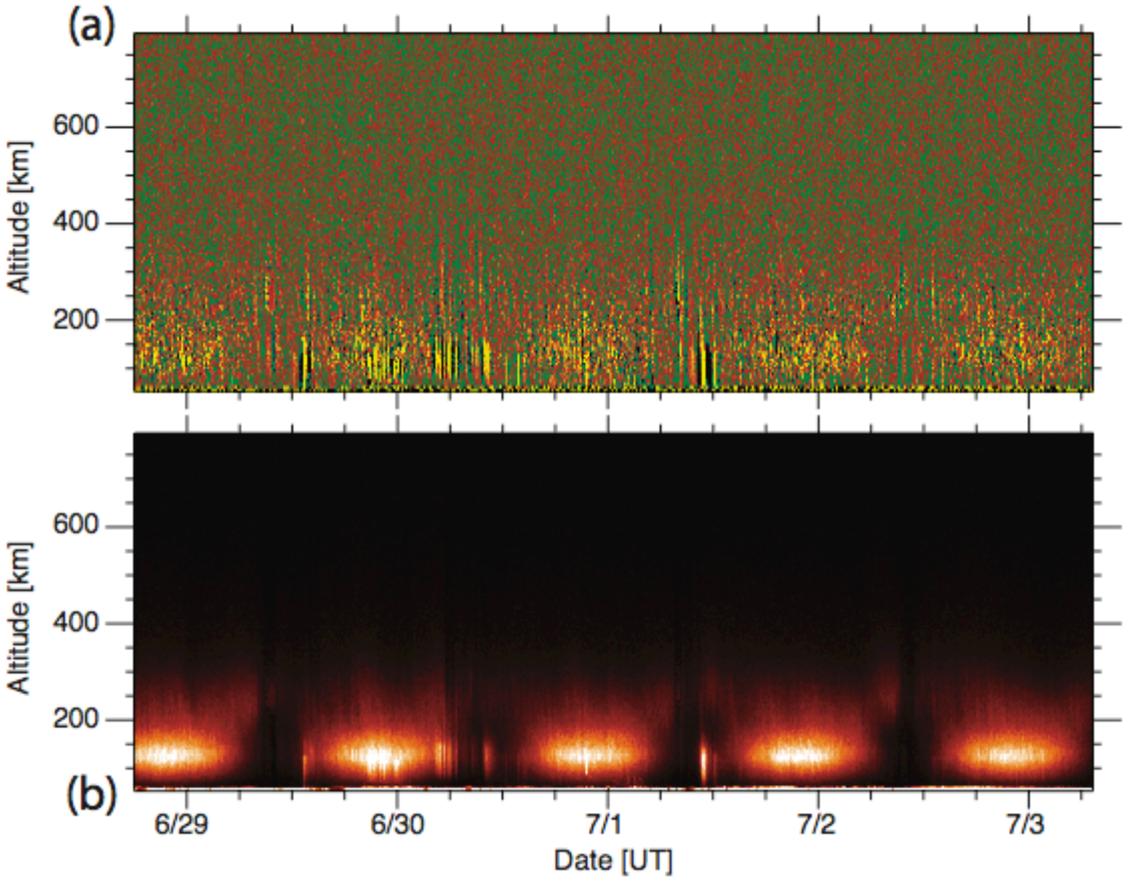

Figure 3.12. Processed (a) and original (b) plots of electron concentration observed at Poker Flat, Alaska near summer solstice on June 28th to July 3rd, 2007. The COFIs can be seen occasionally as vertical strips in the processed plot (a) although some of the stronger vertical stripes e.g. the stripes just before noon on 7/1 are probably better attributed to aurora.

3.4. Multi-Instrument Investigations of the COFIs

In the preceding sections, convincing evidence of the persistent presence of the COFIs at Arecibo and Millstone is presented. Although these results do provide spectacular proof of the existence of the COFIs, they only give vertical and temporal information and are limited to the ionospheric plasma. To understand the COFIs better, it is useful to examine observations from a variety of instruments. This multi-instrument search for the COFIs had varying degrees of success depending on the instruments studied. The most relevant of these observations are presented in this Section.

A logical place to begin our multi-instrument search is the place where the COFIs were first discovered – Arecibo. On the grounds of the Arecibo Observatory, the Penn State All-Sky (Airglow) Imager (PSASI) and a microbarograph have been recording data since 2003. The microbarograph operates continuously and the imager observes on most clear nights.

3.4.1. Airglow Imager Observations

An airglow imager is essentially a camera equipped with an all-sky lens and a frequency-specific filter that looks upward at the ionosphere. Only light at a specific frequency can penetrate the filter and this frequency is characteristic of the light emitted by one of several excited-state atoms or molecules that typically reside in the ionosphere. Depending on the filter pass-frequency, there are several such emissions that an imager can observe, each corresponding to an altitude in the upper atmosphere where the constituents that are needed to provide an ample photon flux for the observation are present. The airglow imager thus enables the observer to see changes in the ionospheric plasma concentration, because the concentration of the necessary excited particle is dependent on the concentration of the required constituents. As the emissions owing to the chemical reactions are quite faint when compared with sunlight, airglow imagers can be used only at night.

Because the COFIs are prominent throughout the bulk of the F2-region, an ideal filter would allow emissions from that altitude. A filter-pass frequency of 630.0 nm, corresponding to the light emitted by the presence of excited atomic oxygen, is ideal for this task. Excited atomic oxygen is present in abundance at an altitude of around 250 kilometers and occurs because of the following two-step reaction. First, a positively charged atomic oxygen ion (typical of the F2 layer) passes its charge to an O_2 molecule in a process termed charge exchange:

$$O^+ + O_2 \longrightarrow O_2^+ + O$$

Then, the positively charged O_2 ion combines with a free electron to produce the excited, 630.0 nm emitting an oxygen atom O^* and a normal oxygen atom in a process called dissociative recombination:

$$O_2^+ + e^- \longrightarrow O^* + O$$

The dissociative recombination process leaves excess energy in the electronic states of atomic oxygen, which results in emission of the 630.0 nm optical emission. The exact height of the 630.0 nm-emitting layer varies with the presence of the necessary constituents. The airglow concentration actually forms a Gaussian distribution in altitude that tends to be centered at a height of around 250 kilometers with a standard deviation of roughly 50 kilometers e.g. [*Shiokawa et al.*, 2003].

Our PSU airglow imager (PSASI) has been recording 630.0 nm and other wavelength observations for most clear nights since 2003 [*Seker et al.*, 2007]. One such clear night occurred on the night of March 22, 2004, a night when the Arecibo ISR was recording the data shown in Figures 3.1 and 3.2. With this fortunate coincidence, we were able to compare the ISR observations directly with the local imager results to try to get a picture of the COFIs. Figure 3.13 shows a series of March 22nd 2004 images from PSASI and the Arecibo incoherent scatter radar from the same time. Each image is numbered to designate where it corresponds to the ISR data shown in Figure 3.13(b).

The color scale has been optimized for each image individually and therefore, all depletions (or enhancements) seen in a particular image are relative to the average airglow density in that image. For example, in image 3 of Figure 3.13a, an enhancement is seen directly over the imager (denoted by the red dot). Although the ionosphere is higher in image 3 than in images 6 to 8 as seen in the ISR data shown in Figure 3.13b, the airglow directly over Arecibo in image 3 is enhanced relative to the mean airglow level for that image. When viewed sequentially in movie form, the images show ‘blobs’ of depleted airglow moving from northeast to southwest at speeds ranging from 100 to 300 km/hour and horizontal wavelengths ranging from 100 to 300 km. Please note that this is a single observation and that there are several processes that may be causing these moving airglow depletions. Still, these values for horizontal velocity and wavelength are the best starting point that we have to estimate the true parameter values of the COFIs.

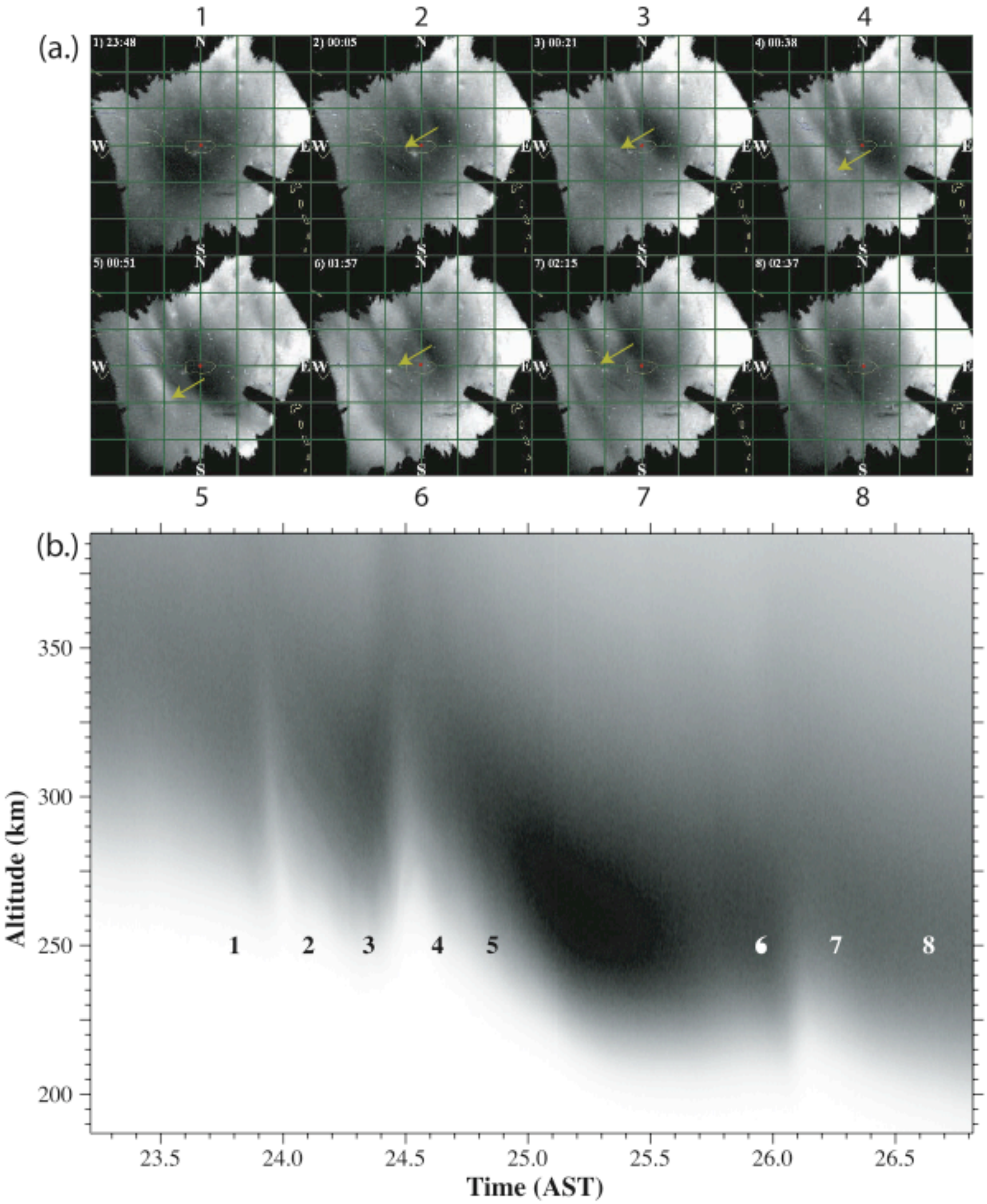

Figure 3.13. Concurrent 630.0 nm airglow images from PSASI (a) and raw Arecibo ISR power profile observations (b) from the night of March 22nd, 2004. Each square in (a) is 200 km across. The red dots in (a) indicate the location of the imager. Each yellow arrow shows the direction of propagation of the depletion that is at its base. The images numbered in (a) each correspond to the times shown in (b). Because airglow tends to be concentrated around 250 km, the numbers on (b) have been placed in the likely location that the images in (a) display.

3.4.2. Arecibo Microbarograph Observations

A microbarograph is a device that measures atmospheric pressure with accuracy better than one millibar. We have been operating a microbarograph at Arecibo and it has been measuring the atmospheric pressure at ground level once per second for the past four years. These data were inspected for evidence of consistent atmospheric pressure oscillations at frequencies similar to those of the COFIs. Figure 3.14 shows the atmospheric pressure spectra as measured by the Arecibo microbarograph for (a) 2004, and (b) 2005. Although tidal harmonics up to the 10^{th} harmonic (2.4 hrs period) in 2004 and the 9^{th} harmonic (2.7 hrs period) in 2005 are significant—note that the 8^{th} harmonic at 3 hrs period is absent in both datasets—there does not appear to be any significant tidal harmonic activity near 1 hr period in these results although some excess energy grouped at 1-2 hrs period is present in the 2004 data. The lack of significant above-noise background, ground-level wave energy at, or near 1 hr period in the Figure 3.14 results suggest that the COFIS observed in the ISR are not due to tidal harmonic energy—as visible at ground-level— 'leaking' into the upper thermosphere.

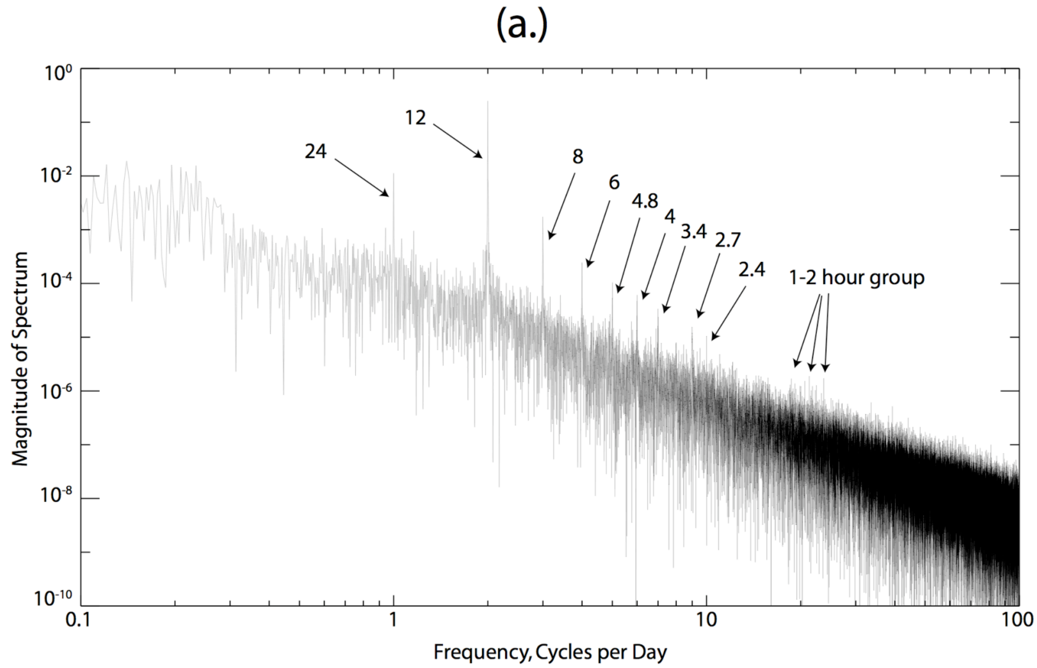

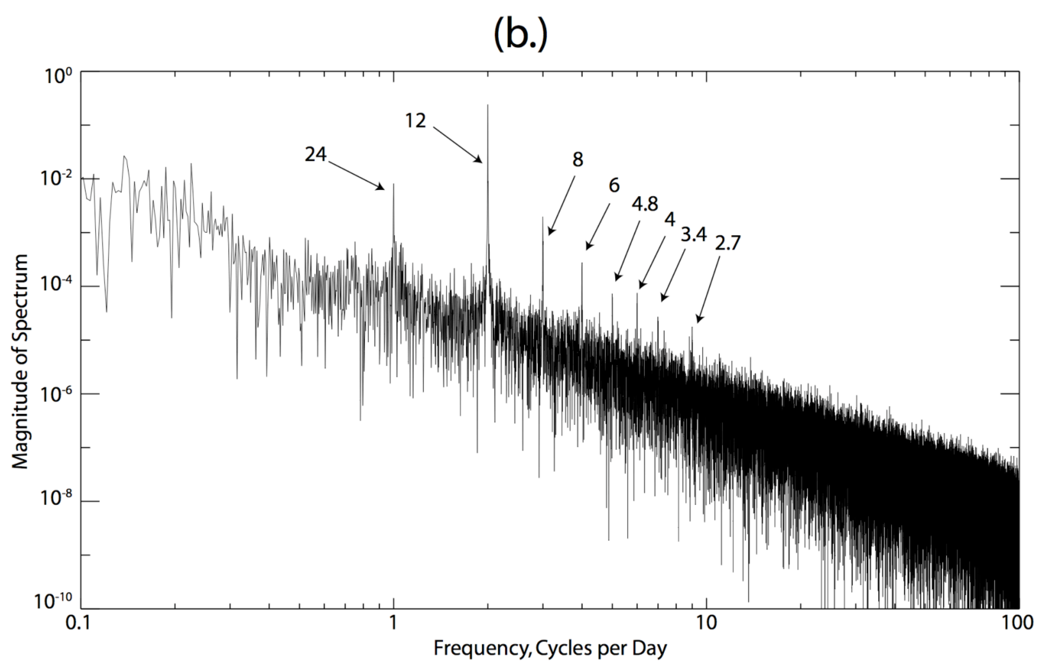

Figure 3.14. Barometric pressure power spectrum for 2004 (a.) and 2005 (b.), with tidal periods shown in hours. The energy in the 1-2 hour group in 2004 (panel a.) may be responsible for some of the wave activity seen in the ISR data. There is no such spectral group in the 2005 (panel b.) data, however. Spectra for 1-3 month periods centered on the Figure 3.1 observing periods do not reveal above noise-level energy in the 1-2 hour period range.

3.4.3. GOES Satellite Observations

Several factors point to the possibility that the COFIs may not be due to acoustic-gravity waves and are actually caused by oscillations of similar frequency in the magnetosphere. This and other scenarios for the COFIs are examined extensively in Chapter 4. Figure 3.15 presents two separate days of observations taken by the Arecibo ISR along with those taken by the Geostationary Operational Environmental Satellites (GOES) numbers 10 and 12, and the Advanced Composition Explorer Satellite (ACE) for a period during which we had Arecibo ISR data – September 22-23, 2005 – see Figure 3.8.

The GOES satellites are positioned over the Earth's equator in geostationary orbit. That is, each satellite always remains over nearly the same geographic location on the Earth's surface. The satellites are at the geosynchronous (also known as the Clarke) height of approximately 35,786 kilometers above mean sea level, putting them firmly outside the ionosphere but well within the magnetosphere. GOES-10 and GOES-12 operate at longitudes of 135° W and 75° W, respectively. Note that the location of GOES-12 is longitudinally similar to that of Arecibo, which is at 66.8° W. Each of these satellites is equipped with several instruments, including a magnetometer. The green and red line plots in Figure 3.15 are high-pass filtered in the same manner as each constant altitude strip of the Arecibo ISR data, as outlined in Sections 3.1 and 3.2 and show total magnetic field strength from GOES-10 and GOES12, respectively. Both of these plots show a *consistent* quasi-periodic variation on the order of 45 minutes, evocative of the COFIs. Notice the strong periodicity of the GOES results, and contrast this consistent oscillation with the more chaotic and only somewhat periodic nature of the Arecibo data. It is only the vertical coherence of the Arecibo data as seen in Figures 3.2, 3.3, 3.8, 3.9, and 3.10 that truly articulate the waves. The periodic nature of the GOES results makes the magnetic oscillations they observe a possible candidate as a source for the COFIs. That these fluctuations may be related to or even be the source of the COFIs is examined in Chapter 4. A cross-correlation between the each of the high-pass filtered GOES magnetometer results with those from 300 km above Arecibo (both in terms of power profile deviation and percent deviation from the background) failed to demonstrate a quantifiable link between the two, however. Cross-correlations were also performed between the high-passed GOES magnetometer results and similarly high-passed results from a number of ground-based magnetometers including the magnetometer at San Juan, PR near Arecibo. These cross correlations also failed to demonstrate a quantifiable link.

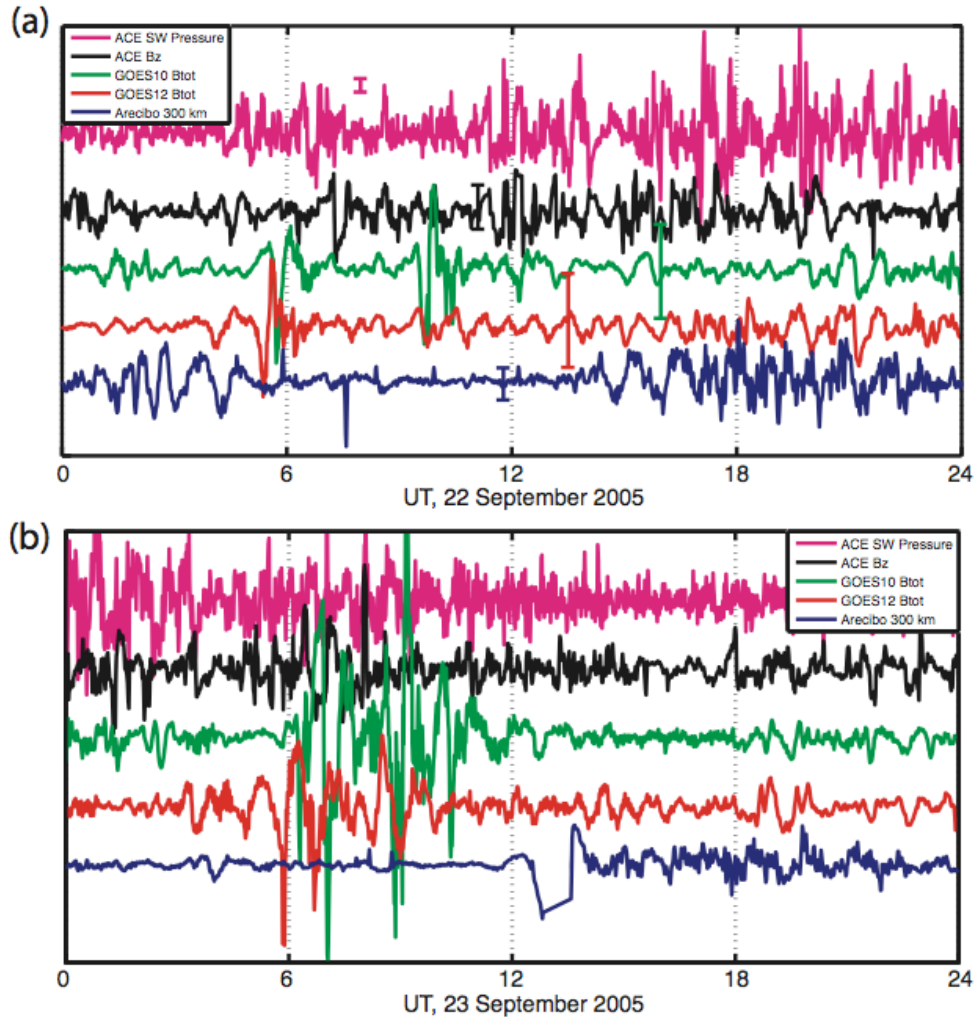

Figure 3.15. All data shown here have been processed (high-pass filtered) as per Sections 3.1 and 3.2. The Figure shows concurrent high-pass filtered observations of (top to bottom) the solar wind pressure (ACE), the solar wind vertical magnetic field, B_z (ACE), the total magnetic field at geosynchronous orbit at the equator with longitudes of 135° W (GOES-10) and 75° W (GOES-12), and ISR signal temperature at 300 km altitude (Arecibo ISR) for 22 September (a) and 23 September (b), 2005. The 'I' bars on the top Figure show what a 10% deviation relative to the background is for each of the measurements.

3.4.4. ACE Satellite Observations

The discovery of oscillations with the appropriate periodicity in the GOES magnetometer results led to the search for similar oscillations further upstream in the process i.e. in the solar wind. The Advanced Composition Explorer Satellite (ACE) does not orbit the Earth but actually orbits about a sun-Earth gravitational balance point called the L1-point some 1.5 million kilometers towards the sun. Here it records data on the solar wind well upstream of the Earth and outside the Earth's protective magnetosphere. Both the magnetic field and the solar wind dynamic pressure were obtained from ACE and the processed results for 22-23 September 2005 are presented in Figure 3.15 as the black and pink lines, respectively. ACE is equipped with a magnetometer so that the magnetic field was obtained directly. The solar wind dynamic pressure, *P,* had to be calculated from the solar wind speed and density using: $P = \rho v^2$; where ρ is the solar wind particle concentration at ACE, and v is the solar wind velocity, however. Although the ACE plots do show some oscillations of the appropriate period from about 1200 UT on September 22nd until around 1100 UT on September 23rd, these fluctuations are not as consistent as those for the GOES magnetic field nor do they seem to occur throughout the entire data set. A full discussion of this result is given in Chapter 4.

4. Discussion

Spatially coherent fluctuations (COFIs) were observed ubiquitously in ISR observations from both the Arecibo Radio Observatory and the Millstone Hill Observatory. Range-time-intensity plots of the COFIs all display a negative phase progression (slope) and gradual increase in vertical wavelength (slope) with height from just over ten kilometers in the lower F1-region to hundreds of kilometers above the F2 peak. This altitude coherence is a testament to the validity and existence of these waves for, as seen in Figure 3.4, the applied signal processing does not induce any false vertical structure. In the Arecibo ISR observations, the COFIs had periods ranging from around 25 to 60 minutes. Features evocative of the COFIs also were observed by other radars, airglow imagers, GPS receiver networks, and satellite-borne instrumentation. Because these other instruments have differing observational capabilities, and because a direct link is as yet *unproven*, the reader is advised that any inferences about the COFIs made from these instruments have to be considered *cautiously*.

Horizontal properties of the COFIs cannot be gleaned from the vertical pointing ISR observations of Arecibo and Millstone. By searching for similar-looking structures in data from other instruments and taking those values as an estimate, one may infer these properties. Of course, this assumes that the phenomena observed by other instruments - i.e. airglow imagers and GPS networks - are indeed the COFIs. Assuming this to be true leads to the COFIs have horizontal wavelengths ranging from 100 to 1000 km corresponding to the minimum value reported from the Arecibo imager by *Livneh et al.* [2008], and the maximum daytime value reported by *Tsugawa et al.* [2007]. The GPS-TEC results of *Tsugawa et al.* [2007] display a velocity of 360 to 720 km/hr towards the *southeast* for the Medium-Scale Traveling Ionospheric Disturbances (MSTIDs) that they observed over North America. For the waves that they observed using the Japanese MU radar, *Oliver et al.* [1997] remark, "On average, the horizontal phase trace speed remains near 240 m/s (864 km/hr) for all periods inspected (40-130 min)." The disparity in these results may be due to differences in what is observed by the various instruments or that the researchers are observing a different phenomenon. Thus we are left with a fairly wide range of velocities for the COFIs. As a best guess from sifting through the literature and giving extra weight to our Arecibo airglow observations, the most likely ranges are a horizontal wavelength of 100 to 400 km and horizontal speeds of 100 to 450 km/hour, with the COFIs almost always traveling southward and especially to the southwest in the northern hemisphere.

The COFIs appear to be present at mid-latitudes regardless of season as seen in the four Arecibo data sets presented in Chapter 3. These observations are taken from near spring equinox (22-24 March 2004), summer (5-7 June 2005), autumnal equinox (21-25 September 2005), and mid/late autumn (17-21 November 2005). There does not appear to be any noticeable difference between these four seasonally different observations of the COFIs. Of course, four observations do not prove a lack of seasonal dependence conclusively, only that there is no indication of such a variation.

Unfortunately, all of the Arecibo Observations were taken during times that were quiet geomagnetically and therefore had a low geomagnetic index K_p. Hence nothing can be said about the effect of K_p on the COFIs at Arecibo except that they do exist consistently during low K_p. Data from more a geomagnetically active period were obtained from Millstone Hill, however, and so a comparison of COFIs at high and low K_p

was made. The somewhat surprising result was that the COFIs were stronger and more distinct during elevated K_p than during quiet times. This result would tend to imply that the COFIs would be observed even more strongly at Arecibo during periods that are more active than those studied when such data become available as we approach the next solar maximum in 2012.

The COFIs apparently exist over a vast geographic area. Millstone Hill and Arecibo are separated by over 2500 km, and the COFIs are consistently observed at both. And, although uncertainty remains, the COFIs may have been detected by other instruments as well. It is likely that the COFIs also were observed over Japan with the MU radar by *Oliver et al.* [1997]. Numerous accounts of airglow images displaying COFI-like phenomena are available from geographically diverse mid-latitude locations e.g. [*Garcia et al.*, 2000; *Shiokawa et al.*, 2002; *Taylor et al.*, 1998]. Therefore, it seems likely that the COFIs extend throughout the mid-latitudes. An interesting observation is given by *Tsugawa et al.* [2007], who found that the amplitude of the MSTID bands that they consistently observe at mid-latitudes (over the continental United States of America) *increases* as the waves propagate southward.

It is more difficult to determine the existence of the COFIs at high and low latitudes. High-latitude data sets are rife with transient observations of MSTIDs. Whether these are in fact the COFIs but can only be observed intermittently because of the limitations of the observing instruments is an open question. Observations from the high latitude of Poker Flat, Alaska are shown in Figure 3.12. There certainly are waves present there, but the poor signal-to-noise ratio makes it difficult to determine if they are always present and whether they resemble the phenomenon observed at Arecibo and

Millstone. Observations of similar but more transient structures have been made at high latitudes in North America with the SuperDARN group of radars by *Bristow and Greenwald*, [1995; 1996]; *Bristow et al.* [1994]; *Bristow et al.* [1996]; and *Samson et al.* [1990]. Interestingly, *Bristow et al.* [1996] found that the waves they observed were more prevalent in winter than in summer, with a probability of 0.8 of seeing waves within a 2-hour period in the winter compared with just a 0.4 probability in the summer. The waves that they observed had periods of 20-50 minutes with horizontal wavelengths between 200 and 450 km and propagation speeds of less than 200 m/s. These values are comparable to those obtained with the airglow imager results from Arecibo that were shown in Figure 3.13. Observations of MSTIDs over northern Europe using the EISCAT radar abound e.g. [*Hocke et al.*, 1996; *Kirchengast et al.*, 1996]. A modeling study by *Kirchengast et al.* [1996] demonstrated that these MSTIDs showed good matching with thermospheric AGWs. These observations *suggest* that the COFIs could be a high-latitude phenomenon as well as a mid-latitude one and point towards aurorally generated AGWs as their source.

No observations were obtained from low latitudes. Several papers may offer some insight, however. *Shiokawa et al.* [2002] used a combination of airglow imaging and GPS-TEC observations to show that the MSTIDs observed over Japan do not propagate to lower latitudes beyond 18° magnetic latitude for the period studied. Somewhat in contrast, *Candido et al.*'s [2008] statistical study of MSTIDs over a low southern latitude airglow imager at Cachoeira, Brazil (22.7°S, 45.0°W, -13.2° mag lat) demonstrates that MSTIDs do penetrate to at least the -13.2° magnetic latitude where their imager is located, but rather infrequently. They see MSTIDs on 11% of the nights during low solar activity, 3% during medium solar activity, and never during high solar activity. The F10.7 index was used to classify the solar activity and K_p was below 2 for all of their observations. Regardless of the conditions, the MSTIDs were observed too sporadically there to be potential COFIs and are likely due to locally generated AGWs.

Thus we are left with a picture of waves likely present at all longitudes that propagate equatorward possibly all the way from high-latitudes down to the lower mid-latitudes but that are absent at low-latitudes. The waves may (again these observations must be treated cautiously) increase in amplitude as they travel through the mid-latitudes as demonstrated by *Tsugawa et al.* [2007] but begin to attenuate in the lower mid-latitudes and finally disappear around 18° magnetic latitude [*Shiokawa et al.*, 2002]. Although this latitude dependency has to be accepted only timidly because the observations may be of differing phenomena, it offers clues to the source and nature of the COFIs. Although the nature and source of the COFIs are unknown, the three most likely explanations are examined in the coming pages. The first is the traditional explanation for MSTIDs, that they are caused by Acoustic-Gravity-Waves (AGWs) launched from the auroral zone. The second is that they are due to AGWs that are generated locally. Lastly, there is a completely non-AGW explanation; that the COFIs are caused by electro-dynamic coupling of magnetic field oscillations observed in the magnetosphere.

4.1. Aurorally Generated Acoustic Gravity Waves Hypothesis

The traditional explanation for MSTIDs is that they are passive plasma imprints of aurorally generated Acoustic-Gravity-Waves created in the high-latitude thermosphere through both Joule heating and the Lorentz force [e.g. [*Francis*, 1975], [*Hocke and Schlegel*, 1996]]. [*Bristow and Greenwald*, 1996; *Bristow et al.*, 1994; *Bristow et al.*, 1996] have repeatedly found AGWs and AGW sources present in the high-latitude ionosphere. Modeling results e.g. [*Kirchengast*, 1996; *Kirchengast et al.*, 1996] show strong agreement between this scenario and TIDs observed by the EISCAT radar, features that are morphologically similar to the COFIs which we observe. For the COFIs to be due to aurorally generated thermospheric AGWs however, the AGWs must travel from the auroral zone to Arecibo. There is some uncertainty over whether or not this is possible. *Vadas* [2007] shows that gravity waves with the observed parameters will dissipate less than 1000 km from their source. In contrast, *Mayr et al.*, [1990] show that gravity waves could propagate large distances in either of two modes. According to *Mayr et al.*, waves might propagate horizontally through the thermosphere, being ducted by the temperature gradient in the mesopause region, or they might propagate in the ducted Earth-reflected mode, leaking into the upper atmosphere. Note that the work of *Vadas* [2007] involved significantly more sophisticated equations and included the effects of dissipation to a much greater extent than the much earlier work of *Mayr et al.* [1990] and thus *Vadas'* work is more likely to be valid – i.e. AGWs dissipate within 1000 km of their source. Regardless of whether AGWs can survive travel over > 5000 km, a fact that disputes the aurorally generated AGW hypothesis is our finding, echoed by the TEC results of *Tsugawa et al.* [2007] that the wave amplitude appears to increase with decreasing latitude. For the auroral AGW theory to be valid, the AGWs would have to grow in amplitude as they propagate away from their source, a growth that does not seem likely.

Before proceeding further, let us investigate whether the vertical properties of the COFIs are consistent with AGWs in general. In Figure 4.1, the vertical wavelength versus altitude estimated for the Arecibo observations near 1600 hrs on 6 June 2005 (see Figure 3.10) is compared with the lossless theoretical result derived from the AGW dispersion relationship given by *Hines* [1965] and elsewhere using appropriate atmospheric parameters given by the atmospheric model MSISE-90 (http://omniweb.gsfc.nasa.gov/vitmo/msis_vitmo.html). Also shown are the modeling results from *Vadas* [2007] for an AGW with horizontal and vertical wavelengths of 200 km and 60 km, respectively, launched at ground level. Although the vertical wavelength variation with altitude exhibited in the data and as modeled by Vadas are quite similar, note that *Vadas* [2007] also gives AGW dissipation heights between 200 km and 300 km for solar minimum (cold thermosphere) to solar maximum conditions, respectively, whereas the COFIs were observed to altitudes in excess of 500 km as seen in figure 3.2.

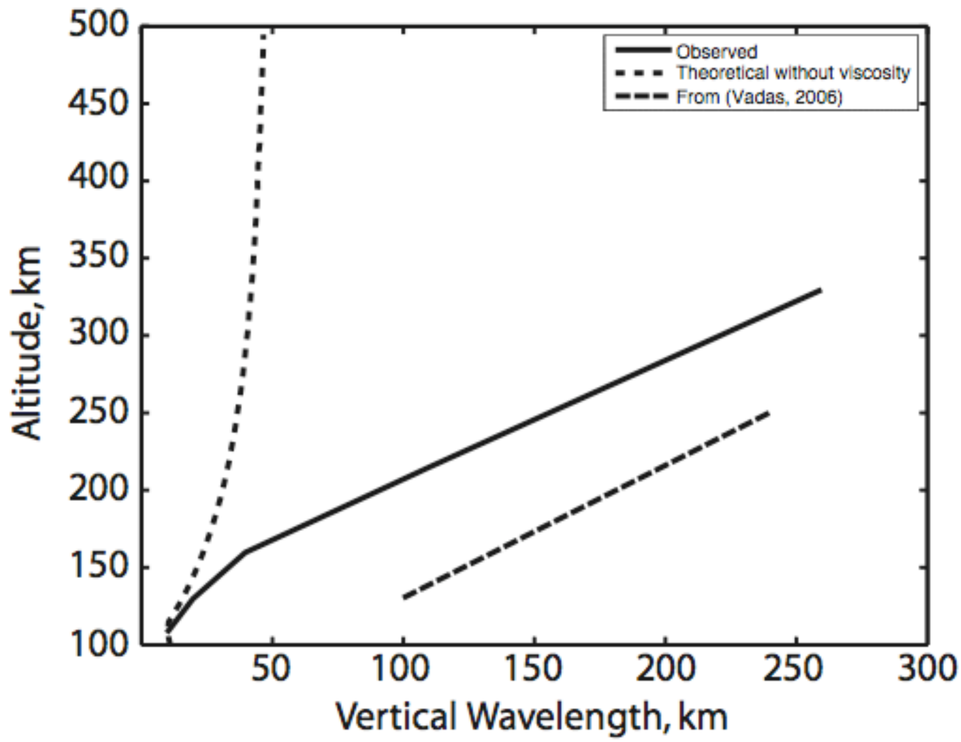

Figure 4.1. A plot of the lossless theoretical (dashed line) [Hines, 1965] and estimated observed (solid line) vertical wavelength versus time for ~1600 UT on 6 June 2005. Also shown are the modeled vertical wavelengths from Figure 2 of [Vadas, 2007] for initial ground-level horizontal and vertical wavelengths of 200 km and 60 km, respectively. Inclusion of kinematic viscosity and thermal diffusion losses leads to the growth of the vertical wavelength relative to the lossless case. The vertical wavelength versus altitude estimated from the data and the viscous modeled results are similar.

Collisional coupling between the neutral atmosphere and the F-region plasma weakens rapidly with increasing altitude and the electrodynamics of waves in the nighttime F-region must obey the electrodynamic equations given by *Perkins* [1973] and elucidated in [*Zhou and Mathews*, 2006; *Zhou et al.*, 2005; *Zhou et al.*, 2006]. In particular, to the extent to which the F-region is decoupled from the E-region, the propagation of wavelike features in the F-region is enhanced to the southwest and northeast while damped to the northwest and southeast, thus providing a filtering mechanism as well as a possible amplification mechanism that certainly influences what we observe with both the ISR and the all-sky camera systems. Further, note that the F-region plasma is incompressible for motions parallel to the geomagnetic field. Thus as the neutral atmosphere AGW forcing of the plasma decouples at the base of the F-region due to decreasing collision frequency and also due to altitude progressive AGW losses, the field-aligned plasma motions at the decoupling altitude are imposed on the entire plasma along that flux tube. Thus, for the Arecibo dip angle near 45º, the horizontal AGW wavelength (as reflected in B-field parallel motions and thus raising/lower of the plasma along each flux tube) at the effective forcing altitude is mapped to the observed vertical motions and thus vertical wavelength. It is unclear if this effect is observed in our data. The observed vertical wavelengths above 300 km appear to remain constant at 200-300 km, however. Note that the Arecibo observations cut across the **B**-field at an angle of 45° and thus show plasma motions that may represent different features at the base of the field line. This would map the horizontal structure of the AGWs to the vertical in the ISR observations.

The ISR results show consistent evidence of the quasi-periodic COFIs, but auroral activity is much more sporadic. Thus, for the aurora to be the source of the phenomenon, the COFIs would have to be band-pass filtered by a tuned thermosphere-ionosphere system. Such a scenario has been modeled successfully by *Millward* [1994] using the Sheffield/UCL coupled ionosphere-thermosphere model. They found that temporally random auroral bursts launched AGWs with preferred periods "strongly biased towards 40-50 minutes," a result that fits very well with our observations. Unfortunately, the low resolution of the model used by *Millward* [1994] casts some doubt as to their applicability to the COFIs. In conclusion, although the consistency of the COFIs may not favor an auroral origin, it need not preclude it either.

AGWs of the periods and horizontal wavelengths of the COFIs dissipate at heights of ~200 km e.g. *Vadas* [2007], although the COFIs are seen up to ~750 km in the ISR data (Figures 3.2b and 3.10). It is therefore unlikely that wave observations at heights greater than 200 km are due to in situ passive plasma tracing of AGWs, even if the COFIs are indeed caused by AGWs. Rather, there must be some purely electrodynamic effects moving the plasma at heights greater than 200 km. A possible scenario is that the AGW-induced periodic plasma motions in the lower F-region push the higher plasma up and down the geomagnetic field lines. At these heights, plasma motion becomes incompressible along the geomagnetic field lines. Thus, what we observe above 200 km is the motion of the plasma along the field lines and not direct tracing of AGWs but below ~200 km we progressively see the AGWs more directly. It is important to note that Large-Scale traveling ionospheric disturbances can easily travel from the auroral zone to Arecibo, but these are sporadic events that are clearly not the same phenomenon as the COFIs.

4.2. Locally Generated AGWs Hypothesis

Because there is uncertainty as to whether the COFIs are due to aurorally generated AGWs, two other possibilities suggest themselves: non-auroral AGWs and a completely non-AGW hypothesis. Here, the locally generated AGW explanation is explored with the help of *Djuth* [2009]. Because the Arecibo observations are the most compelling, for a local AGW hypothesis to be valid, a source near Puerto Rico must be located. *Thome and Rao* [1969] performed ray tracing calculations and estimated that the local source of the Arecibo AGWs was at a ground distance of ~550 km. This calculation was performed under the assumption that the source was at tropospheric altitudes. AGWs can be generated locally by the passage of tropospheric storms e.g. [*Boska and Sauli*, 2001; *Sauli*, 2001]. Given the size of the current database, it is difficult to argue that tropospheric storms are always present at just the right range (e.g., 500–600 km) to account for all observations. A typical observation period is 48 hours, and so a storm would have to be active day and night for a relatively long period of time. It is possible that trade winds flowing over orographic features on a Leeward Island (e.g., Barbuda) could give rise to AGWs. Barbuda is in the correct location to generate AGWs above Arecibo, but the tallest feature on this island is a hill in the highlands that is only 42 meters above sea level. If trade winds blowing across the highland region of Barbuda are hypothesized as the AGW source, then there should be major seasonal variations in the thermospheric waves seen at Arecibo, but that is not the case. The trade winds in this region change direction depending on the month of the year. During the months of April through June, the average Trade Winds at Barbuda are in the direction of Arecibo, whereas during the months of July through March they are not. *Maximenko et al.* [2008] show that small (~2 cm in height) stationary striations separated by ~400 km are present in most regions of the world's oceans. The ocean surrounding Puerto Rico from the northeast to the southwest contains these jet-like features at the appropriate distance for AGW generation. The striations are located in a large region that would allow trade winds to blow across them year round in the direction of Puerto Rico. Model calculations are required to determine whether the speed of the Trade Winds (5−7 m/s in regions of interest) are large enough to initiate AGW propagation into the Arecibo thermosphere.

Large tsunamis (50-60 cm amplitude on open water, 300–400 km in wavelength) such as the Sumatra tsunami of December 26, 2004 produce internal gravity waves in the neutral atmosphere that give rise to large disturbances in the overlying ionosphere [*Occhipinti et al.*, 2006]. Even very small tsunamis (1-2 cm amplitude on open water) generate significant TIDs that are readily observable with a Global Positioning Satellite (GPS) network [*Lognonne et al.*, 2006b; *Lognonne et al.*, 2006a]. Of course, the sensitivity of the Arecibo ISR system is much greater than that of the GPS, and so the existence of such waves above Arecibo would be detected readily. Natural infragravity (infragravity waves have periods of 0.5 to 30 minutes) ocean waves traveling over deep (4 km) water and having periods of ~5-6 min and amplitudes of 1-2 cm have been observed with a few broadband seismographs at the bottom of the Pacific and Atlantic Oceans. (See [*Tanimoto*, 2005] and the references therein.) In the ocean north of Puerto Rico (depths of 5−6 km), these waves would have wavelengths of the order of 66 to 72 km and propagate in a nearly lossless manner. Ocean waves with periods greater than 6 min and therefore longer wavelengths cannot be detected with the deep-water seismographs because of the dominant contribution of the atmosphere at these periods. Thus, the presence of small-amplitude infragravity waves having wavelengths of the order of 100−200 km has yet to be explored. Such waves would refract off the Puerto Rico trench (8,648 m in depth) northeast of Arecibo and potentially give rise to other ocean waves/structures that could either generate AGWs directly or interact with the trade winds to produce the observed thermospheric waves. We are in the process of examining the ocean surface within 500–600 km of Arecibo with the aid of satellite altimetry to determine whether the ocean is a viable source of the waves.

The locally generated AGW hypothesis has the advantage of fitting well with the Arecibo ISR observations. It does not explain why the COFIs were also observed at Millstone however, nor why the COFIs are possibly observed worldwide – over all of North America by *Tsugawa et al.* [2007], over Japan e.g. [*Oliver et al.*, 1997; *Taylor et al.*, 1998], [*Shiokawa et al.*, 2006], and over Australia [*Otsuka et al.*, 2004]. Still, it is possible that the COFIs indeed are generated locally at all of these locations or that something different is being observed at Arecibo than elsewhere, and thus this hypothesis is viable.

4.3. Non-AGW Hypothesis

As discussed above, an AGW-based explanation for these COFIs is certainly possible but suffers from some difficulties. An alternative explanation is that the COFIs are caused by oscillations in the solar wind that couple to the ionosphere via the magnetosphere. GOES-10 and -12 satellite magnetometer data was processed for the periods for which ISR observations from Arecibo were available. Quasi-continuous ~45-minute period fluctuations in the total magnetic field measurements at geosynchronous orbit were discovered. Figure 3.15 shows concurrent high-pass filtered observations of the solar wind pressure and $\mathbf{B_z}$ from the Advanced Composition Explorer (ACE) satellite, the geomagnetic field at geosynchronous altitude from GOES-10 and -12, and incoherent scatter power, which is proportional to electron concentration at 300 km at Arecibo. Notice the consistency of the fluctuations in the GOES results. In this representation, the oscillations in the GOES results are even more consistent than those from Arecibo. In fact, the COFIs are only totally apparent in the Arecibo data when the data are displayed as signal power as a function of altitude and time as in Figure 3.1. The evidence for a link between the oscillations in the magnetosphere given by GOES and those in the ionosphere given by ISR, imager, and TEC observations is examined next.

Villante et al. [2003] examined ground magnetometer data at L'Aquila (AQ, Central Italy, corrected geomagnetic latitude 36.2° N) for the same time interval for which *Kepko et al.* [2002] had shown a link between fluctuations in the solar wind and the magnetosphere. They found that the H-component of the geomagnetic field as observed at AQ showed variations matching those in the SW pressure and in the magnetospheric magnetic field magnitude as measured by GOES-8 and -12. These variations had periods of roughly 30 minutes, similar to the COFIs at Arecibo. This result is a convincing demonstration of a SW-magnetosphere-ionosphere link at this frequency.

Dyrud et al. [2008] inspected 204 minutes of concurrent data from the solar wind (WIND satellite), magnetosphere (GOES), and the ionosphere (Arecibo) to search for coupling of oscillations between them. For their observations, they used both the linefeed and the Gregorian beams of the Arecibo Observatory and pointed them 15° south and north of zenith, respectively to give a horizontal perspective to their observations. They found that 1.7 mHz deviations of about 1% (the COFIs we observe are fluctuations of roughly 5% in electron concentration) in the ionospheric plasma line at the F-region peak observed by both Arecibo beams were concurrent with similar 1.7 mHz oscillations regularly observed in the solar wind and magnetosphere, and that these oscillations propagated from north to south at an apparent speed of 500 m/s. Although the data set they used is too short (204 minutes) to properly examine (at least in the frequency domain) oscillations with the periods of the COFIs (~50 minutes), their results also provide strong evidence of coupling between oscillations in the solar wind and the heart of the Arecibo F-Region. *Kelley et al.* [2003] found that during a magnetic storm, fluctuations in the solar wind of periods similar to those of the COFIs were observed clearly in the E-field of the equatorial ionosphere as measured using the Jicamarca Radio Observatory in Peru. They also "detected the event in other radars in the U. S. chain but not with as much clarity," implying that penetration of periodic oscillations may be stronger at the equator than at higher latitudes. Although the COFIs are a steady state or quiet time phenomenon, the fact that the effects of the solar wind have been observed in the equatorial and mid-latitude ionosphere allows the possibility that the COFIs may in fact be due to solar wind-magntosphere-ionosphere coupling.

The link between ULF fluctuations in the solar wind and those in the magnetosphere has been established. For example, *Kepko and Spence* [2003] convincingly showed that variations in the solar wind pressure forced the magnetopause to move, thereby compressing and expanding the magnetosphere and causing similar, in both time and frequency, variations in the Earth's magnetic field. They found this mechanism to be hold for the often observed frequencies of 1.3, 1.9, 2.6 and 3.4 mHz. More pertinently for the investigation of the COFIs, they found significant Solar Wind (SW) – magnetosphere coupling at frequencies below 1 mHz, namely at 0.1, 0.2, and 0.56 mHz that translate into periods of 167, 83, and 31 minutes, respectively. These frequencies are similar to those of the coherent COFIs observed with the Arecibo and

Millstone Hill radars and suggest that at least the solar wind and magnetosphere are coupled at the relevant frequencies.

Solar wind pressure and $\mathbf{B_z}$ results from the ACE satellite were examined for those periods during which we have Arecibo ISR data. Figure 3.15 shows high-passed ACE data plotted along with concurrent data from GOES and Arecibo. Both the solar wind pressure and the $\mathbf{B_z}$ time series show significant periodicity at the 30 to 60 minute period range, although the pressures seem to contain significantly more high-frequency variability as well. However, neither of the solar wind parameters (i.e. $\mathbf{B_z}$ and dynamic pressure) have the consistent periodicity that is seen in the total magnetic field measurements at geosynchronous orbit by both GOES satellites. One may therefore conclude that there must be some 'filtering' or 'tuning' mechanism that favors the 30 to 60-minute periods as solar wind energy couples to the magnetosphere.

The COFIs exhibit an increase in vertical wavelength with altitude. Although it is true that that this increase is characteristic of AGWs in the thermosphere (e.g. [*Livneh et al* 2007]), the increasing wavelength may also be explained by gradual decoupling between the ions and the neutrals in the lower ionosphere while above ~150 km the plasma motion parallel to **B** is incompressible. Absent large-scale E-fields, the plasma moves strictly along the geomagnetic field lines above around 200 km altitude. Below this altitude, the effects of the neutral atmosphere are progressively more apparent on the plasma motions. Thus, the periodic MSTID-induced motion of the plasma is increasingly "damped" – forced to move horizontally - by the surrounding neutral atmosphere as the altitude decreases into the lower F-region. This process may account for the apparent smaller vertical wavelength at lower altitudes. This process does not, however, account for the fact that COFIs with periods as short as 25 minutes are observed in the lower F-region; while in the upper F-region, only COFIs with periods greater than 50 minutes are observed. This fact tends to favor an AGW explanation, as the ability of an AGW to survive to greater heights is dependent on it having a longer period. Still, it is possible that the COFIs are indeed magnetospherically produced and that the higher frequencies seen in the lower F-region are due to other processes interacting with the COFIs because at these heights, collisions with the neutrals play a significant role.

4.4. Pros, Cons, and Testing of the Three Hypotheses

The three most likely hypotheses are discussed in the previous sections. In this section, the arguments to differentiate between these hypotheses are tabulated and briefly summarized. Any tests that could be used to validate a particular hypothesis are noted in the paragraphs following the associated table. Because the auroral and local AGW hypotheses are each a subset of an AGW explanation, the pros and cons of and AGW-based hypothesis in general are summarized first to avoid redundancy.

Table 4.1. AGWs: Pros and Cons

Pros	Cons
• A link between AGWs and MSTIDs is firmly established in the literature. • Reasonable agreement between COFIs and the dissipative AGW dispersion relationship of Vadas, [2007] – see figure 4.1. • Increasing vertical wavelength with height is typical of thermospheric AGWs.	• Lack of a consistent periodic source. • AGW dissipation – both vertical and horizontal contrasts with large geographic extent of the COFIs. • Plasma motion above ~200 km is decoupled from the neutrals e.g. [Sangalli et al., 2008].[10] • Possible increase in amplitude with decreasing latitude [Tsugawa et al., 2007].

The most compelling arguments for an AGW basis for the COFIs are that AGWs are the overwhelmingly common explanation for TIDs in the literature; and that the increasing vertical wavelength with altitude of the COFIs is successfully predicted by an AGW hypothesis. The vertical wavelength of the COFIs shows a fairly good match with the dissipative AGW dispersion relationship of *Vadas* [2007] as seen in Figure 4.1. These are strong points in favor of the AGW explanation and seem at first glance to definitively confirm it. There are several problems with the AGW hypothesis, however.

The main problems with an AGW explanation are the lack of a viable source and the theoretical fact that medium-scale AGWs cannot survive travel over long distances nor propagate into the upper thermosphere. These problems imply that not only are the AGWs unable to travel from their source to the locations where they are observed, but

[10] The decoupling of neutral and plasma motions above around 200 km does not actually contradict an AGW-based explanation, but it does mean that what is observed at those heights is not a direct imprint an AGW and that an electrodynamic explanation is necessary at these heights.

also that no such source has been identified for them to originate from. Two candidate sources are available, however. The first is heating and collisions caused by auroral processes. The second is a local tropospheric source, most likely AGWs excited by large-scale ocean waves. Each of these sources has advantages and disadvantages and these are outlined in Table 4.2.

A true comparison of the predictions of an AGW-based hypothesis with the observed COFIs would require an accurate model that combines for two factors that cause the plasma imprint of an AGW in the thermosphere to deviate from the ideal, lossless AGW dispersion relationship of *Hines,* [1960]. The first such factor is the dissipative effects of kinematic viscosity and thermal diffusivity as modeled by *Vadas* [2007]. The second factor is the decreasing degree of neutral to plasma coupling with increasing altitude in the ionosphere. At the time of this writing, no such model exists [*Rishbeth*, 2008; *Richmond*, 2008]. To be useful in testing the COFIs, a model requires a spatial resolution of better than around 50 km and a time resolution better than around 5 minutes.

Determining the distance traveled through the thermosphere by an AGW of a given size is also a question that can best be answered by modeling. At this time, the prevailing thought in the thermospheric AGW community indicates that AGWs of the scales of the COFIs can travel about 2000 km before dissipating e.g. [*Vadas*, 2007].

Table 4.2. Aurorally Generated AGW Hypothesis: Pros and Cons

Pros	Cons
• Often cited as source for TIDs in the literature. • Explains apparent mid-latitude ubiquity of COFIs. • Not a quasi-periodic source. • Matches with southern direction of travel as reported in airglow imagers and GPS-TEC. • Source is distant enough to produce the planar wavefronts seen in airglow imagers and GPS-TEC.	• Not a consistent quasi-periodic source. • Horizontal dissipation; Medium-Scale AGWs theoretically cannot travel from the auroral zone to Arecibo.

Auroral processes could be seen as a viable source for COFIs at least within the AGW dissipation range if they could be shown to preferentially produce AGWs with periods of around 45 minutes as was reported by *Millward* [1994] using the Sheffield/UCL coupled ionosphere-thermosphere model. The problem with applying *Millward's* result to investiaging the COFIs is that the model has a resolution that is too low to investigate the COFIs and is more appropriate for Large-Scale Traveling Ionospheric Disturbances (LSTIDs). Attempting such a test with a higher resolution model would be useful.

Table 4.3. Locally Generated AGW Hypothesis: Pros and Cons

Pros	Cons
• The observed negative phase progression with altitude is consistent with AGWs propagating upwards from the local troposphere. • Good match with ray tracing calculations [*Djuth*, 2009].	• No proven local source. • Doesn't explain broad geographical range of the COFIs nor the large and planar wavefronts observed in airglow imagers and GPS-TEC.

The locally generated AGW hypothesis could be essentially eliminated if the large-scale wave features seen in dense and wide GPS-TEC observations or simultaneous airglow imager observations can be definitively linked to the ISR observations of the COFIs. AGWs generated locally near Arecibo (or any other observatory) would not create ionospheric structures that have long wavefronts (>2000 km) and travel equatorward in a quasi-coherent manner.

To better understand whether the COFIs are caused by AGWs, a valuable test would be to obtain very accurate Incoherent-Scatter-Radar data from Arecibo using the coded long-pulse (CLP) radar technique of *Sulzer*, [1986] yielding extremely accurate plasma line based electron concentration profiles plasma enhanced by daytime photoelectrons (PEPL) [*Djuth et al.*, 1994] and compare this with a new and updated AGW-ionosphere coupling model discussed above.

Table 4.4. Magnetospheric Oscillations Coupling Hypothesis: Pros and Cons

Pros	Cons
• Fluctuations observed by GOES magnetometers are an observable quasi-periodic source. • GOES fluctuations are consistently periodic, even more so than those at Arecibo – see Figure 3.15. • Frequency of oscillations at GOES matches very well with that of the COFIs seen at Arecibo.	• Magnetosphere-Ionosphere wave coupling at mid-latitudes has only limited support in the literature e.g. [Villante et al., 2003]. • Does not predict the increasing vertical wavelength and period with height of the COFIs as observed by the ISR. • Cross-correlation of GOES magnetometer results with ISR and ground magnetometers did not confirm link.

The consistent ~45-minute period oscillations observed by the GOES magnetometer are the only consistent candidate source with the appropriate period that we have observed. Cross-correlations between the ~45 minute fluctuations in the GOES magnetometer results have been performed with each of the ISR data sets as well as with several ground based magnetometers including at San Juan, Puerto Rico nearby to Arecibo. None of the cross-correlations verified a significant quantifiable relationship between the GOES oscillations and the ionosphere.

Magnetic field data from various locations within the magnetosphere could be examined to see if the ~50-minute oscillations observed at GOES are present there as well. If so, it is more likely that the oscillations represent a pulsing of the magnetic field lines as a whole. If this is true, the oscillations seen by GOES will also exist in the ionosphere because the magnetic field lines will be oscillating there as well.

4.5. Closing Thoughts

The COFIs now appear to be a widespread phenomenon but although it is still uncertain what they are or where they come from, we have made significant progress in understanding the possibilities. This phenomenon has a global reach and solving this mystery may have implications for our overall understanding of the ionosphere. Each of the three hypotheses for the source of the COFIs discussed in this chapter seem on the one hand highly promising but on the other hand appear to be inconsistent with theory and observations. Further observations can help to determine which of the three hypotheses is correct.

References

Banks, P. M., and G. Kockarts (1973), *Aeronomy - Part A,* Academic Press, New York and London.

Boska, J., and P. Sauli (2001), Observations of gravity waves of meteorological origin in the F-Region ionosphere, *Physics and Chemistry of the Earth*, *26*, 425-428.

Bristow, W. A., and R. A. Greenwald (1995), Estimating gravity wave parameters from oblique high-frequency backscatter: Modeling and analysis, *Journal of Geophysical Research*, *100*, 3639-3648.

Bristow, W. A., and R. A. Greenwald (1996), Multiradar observations of medium-scale acoustic gravity waves using the Super Dual Auroral Network, *Journal of Geophysical Research*, *101*, 24499-24511.

Bristow, W. A., R. A. Greenwald, and J. C. Samson (1994), Identification of high-latitude acoustic gravity wave sources using the Goose Bay radar, *Journal of Geophysical Research*, *99*, 319-331.

Bristow, W. A., R. A. Greenwald, and J. P. Villain (1996), On the seasonal dependence of medium-scale atmospheric gravity waves in the upper atmosphere at high latitudes, *Journal of Geophysical Research*, *101*, 15685-15699.

Campbell, W. H. (2003), *Introduction to Geomagnetic Fields*, Cambridge University Press, Cambridge.

Canavero, F. G., and F. Einaudi (1987), Time and space variability of spectral estimates of atmospheric pressure, *Journal of the Atmospheric Sciences*, *44*, 1589-1604.

Candido, C. M. N., A. A. Pimenta, J. A. Bittencourt, and F. Becker-Guedes (2008), Statistical analysis of the occurence of medium-scale traveling ionospheric disturbances over Brazilian low latitudes using OI 630.0 nm emission all-sky images, *Geophysical Research Letters*, *35*, L17105, doi:17110.11029/12008GL035043.

Cevolani, G., Dardi, A., Formiggini, C., Kingsley, S. P., and H. G. Muller (1983), Wave motions in the lower thermosphere during the energy budget campaign 1980 from three locations in the northern hemisphere, *Il Nuevo Cimento*, *6C*, 271-295.

Cole, K. D. (1971), Electrodynamic heating and movement of the thermosphere, *Planetary and Space Science*, *19*, 59-75.

Djuth, F. T. (2009), *Personal Communication*.

Djuth, F. T., M. P. Sulzer, and J. H. Elder (1994), Application of the coded long pulse technique to plasma line studies of the ionosphere, *Geophysical Research Letters*, *21*, 2725-2728.

Djuth, F. T., M. P. Sulzer, J. H. Elder, and V. B. Wickwar (1997), High-resolution studies of atmosphere-ionosphere coupling at Arecibo Observatory, Puerto Rico, *Radio Science*, *32*, 2321-2344.

Djuth, F. T., M. P. Sulzer, S. A. Gonzales, J. D. Mathews, J. H. Elder, and R. L. Walterscheid (2004), A continuum of gravity waves in the Arecibo thermosphere?, *Geophysical Research Letters*, *31*, L16801.

Dyrud, L. P., R. Behnke, E. L. Kepko, M. Sulzer, and S. Zafke (2008), Ionospheric ULF oscillations driven from above Arecibo, *Geophysical Research Letters*, *In press*.

Francis, S. H. (1974), A theory of medium-scale traveling ionospheric disturbances, *Journal of Geophysical Research*, *79*, 5245-5260.

Francis, S. H. (1975), Global propagation of atmospheric gravity waves: a review, *Journal of Atmospheric and Terrestrial Physics*, *37*, 1011-1054.

Garcia, F. J., M. C. Kelley, J. J. Makela, and C.-S. Huang (2000), Airglow observations of mesoscale low-velocity traveling ionospheric disturbances at midlatitudes, *Journal of Geophysical Research*, *105*, 18407-18415.

Harper, R. M. (1972), Observations of a large nighttime gravity wave at Arecibo, *Journal of Geophysical Research*, *77*, 1311-1315.

Hearn, A. L., and K. C. Yeh (1977), Medium scale TIDs and their associated internal gravity waves as seen through height-dependent electron density power spectra, *Journal of Geophysical Research*, *82*, 4983-4990.

Hines, C. O. (1960), Internal gravity waves at ionospheric heights, *Canadian Journal of Physics*, *38*, 1441-1481.

Hines, C. O. (1965), Atmospheric Gravity Waves: A New Toy for the Wave Theorist, *Radio Science*, *69D*, 375-380.

Hines, C. O. (1974), *The Upper Atmosphere in Motion*, American Geophysical Union, Washington, D. C.

Hocke, K., and K. Schlegel (1996), A review of atmospheric gravity waves and traveling ionospheric disturbances: 1982-1995, *Annales Geophysicae*, *14*, 917-940.

Hocke, K., K. Schlegel, and G. Kirchengast (1996), Phases and amplitudes of TIDs in the high latitude F-region observed by EISCAT, *Journal of Atmospheric and Terrestrial Physics*, *58*, 245-255.

Huang, C.-S., S. Sazykin, J. L. Chau, N. Maruyama, and M. C. Kelley (2007), Penetration electric fields: Efficiency and characteristic time scale, *Journal of Atmospheric and Solar-Terrestrial Physics*, *69*, 1135-1146.

Hunsucker, R. D. (1982), Atmospheric gravity waves generated in the high-latitude ionosphere: A review, *Geophys. Space Phys.*, *20*, 293-315.

Kato, S. (2007), Thermosphere, in *Handbook of the Solar-Terrestrial Environment*, edited by Y. Kamide and A. Chian, pp. 221-245, Springer-Verlag, Berlin Heidelberg.

Kelley, M. (1989), *The Earth's Ionosphere, Plasma Physics and Electrodynamics*, Academic Press, New York.

Kelley, M., J. J. Makela, J. L. Chau, and M. J. Nicolls (2003), Penetration of the solar wind electric field into the magnetosphere/ionosphere system, *Geophysical Research Letters*, *30*, doi:10.1029/2002GL016321.

Kepko, E. L., and H. E. Spence (2003), Observations of discrete, global magnetospheric oscillations directly driven by solar wind density variations, *Journal of Geophysical Research*, *108 doi:10:1029/2002JA009676*.

Kepko, E. L., H. E. Spence, and H. J. Singer (2002), *Geophysical Research Letters*, *29*.

Kirchengast, G. (1996), Elucidation of the physics of the gravity wave-TID relationship with the aid of theoretical simulations, *Journal of Geophysical Research*, *101*, 13353-13368.

Kirchengast, G., K. Hocke, and K. Schlegel (1996), The gravity wave-TID relationship: insight via theoretical model-EISCAT data comparison, *Journal of Atmospheric and Terrestrial Physics*, *58*, 233-243.

Lastovicka, J. (2006), Forcing of the ionosphere by waves from below, *Journal of Atmospheric and Solar-Terrestrial Physics*, *68*, 479-497.

Livneh, D. J., I. Seker, F. T. Djuth, and J. D. Mathews (2007), Continuous quasi-periodic waves over Arecibo, *Journal of Geophysical Research*, *112*, DOI: 10.1029/2006JA012225.

Livneh, D. J., I. Seker, F. T. Djuth, and J. D. Mathews (2008), Continuous waves in the ionosphere and their possible sources, *Journal of Geophysical Research*, *In Press*.

Lognonne, P. L., P. J. Artry, F. Garcia, F. Crespon, V. Ducic, E. Jeansour, G. Occhipinti, J. Helbert, G. Moreuax, and P. E. Godet (2006b), Ground-based GPS imaging of ionospheric post-seismic signal, *Planetary and Space Science*, *54*, 528-540.

Lognonne, P. L., R. Garcia, F. Crespon, G. Occhipinti, and E. Alam Kherani (2006a), Seismic waves in the ionosphere.

Mathews, J. D. (1984), The Incoherent Scatter Radar as a tool for studying the Ionospheric D region *Journal of Atmospheric and Terrestrial Physics*, *46*, 975-986.

Mathews, J. D. (1986), Incoherent Scatter probing of the 60-100 km atmosphere and ionosphere, *IEEE Trans. Geosci. Remote Sensing*, *GE-24*, 765-776.

Mathews, J. D., J. K. Breakall, and Ganguly (1982), The measurement of diurnal variations of electron concentration in the 60-100 km ionosphere at Arecibo, *Journal of Atmospheric and Terrestrial Physics*, *44*.

Mathews, J. D., J. K. Breakall, and G. K. Karawas (1985), The Discrete Prolate Spheroidal Filter as a Digital Signal Processing Tool, IEEE Transactions on Acoustics, Speech, and Signal Processing, ASSP-33, 1471-1478.

Mathews, J. D. (1998), Sporadic E: current views and recent progress, Journal of Atmospheric and Solar-Terrestrial Physics, 60, 413-435.

Maximenko, N. A., O. V. Melnichenko, P. P. Niiler, and H. Sasaki (2008), Stationary mesoscale jet-like features in the ocean, Geophysical Research Letters, 35, L08603, doi:10.1029/2008GL033267.

Mayr, H. G., I. Harris, F. A. Herrero, N. W. Spencer, F. Varosi, and W. D. Persnell (1990), Thermospheric gravity waves: observations and interpretation using the transfer function model (TFM), *Space Science Reviews*, *54*, 297-375.

Millward, G. H. (1994), A resonance effect in AGWs created by periodic recurrent bursts in the auroral electric field, *Annales Geophysicae*, *12*, 94-96.

Nicolls, M. J., M. C. Kelley, A. J. Coster, S. A. Gonzales, and J. J. Makela (2004), Imaging the structure of a large-scale TID using ISR and TEC data, *Geophysical Research Letters*, *31*, 2004GL019797.

Occhipinti, G., P. L. Lognonne, E. A. Kherani, and H. Hebert (2006), Three-dimensional waveform modeling of ionospheric signature induced by the 2004 Sumatra Tsunami, *Geophysical Research Letters*, *33, L20104*, doi:10.1029/2006GL026865.

Oliver, W. L., S. Fukao, Y. Yamamoto, and T. Takami (1994), Middle and upper atmosphere radar observations of ionospheric density gradients produced by gravity wave packets, *Journal of Geophysical Research*, *99*, 6321-6329.

Oliver, W. L., Y. Otsuka, M. Sato, T. Takami, and S. Fukao (1997), A climatology of F region gravity wave propagation over the middle and upper atmosphere radar, *Journal of Geophysical Research*, *102*, 14499-14512.

Otsuka, Y., K. Shiokawa, T. Ogawa, and P. Wilkinson (2004), Geomagnetic conjugate observations of medium-scale traveling ionospheric disturbances at midlatitude using all-sky imagers, *Geophysical Research Letters*, *31*, L15803.

Perkins, F. W. (1973), Spread F and ionospheric currents, *Journal of Geophysical Research*, *78*, 218-226.

Philbrick, C. R. (1981), Measurements of structural features in profiles of mesospheric denstiy, in *Hanbook for MAP*, edited by S. K. Avery, University of Illinois, Urbana, Illinois.

Philbrick, C. R., et al. (1985), Density and temperature structure over northern Europe, *Journal of Atmospheric and Terrestrial Physics*, *47*, 159-172.

Richmond, A. (2008), *Personal Communication*.

Rishbeth, H. (2008), *Personal Communication*.

Saito, A., M. NIshimura, M. Yamamato, S. Fukao, M. Kubota, K. Shiokawa, Y. Otsuka, T. Ogawa, M. Ishii, T. Sakanoi, and S. Miyazaki (2001), Traveling ionospheric disturbances detected in the FRONT campaign, *Geophysical Research Letters*, *28*, 689-692.

Samson, J. C., R. A. Greenwald, J. M. Ruohonniemi, A. Frey, and K. B. Baker (1990), Goose Bay radar observations of Earth-reflected atmospheric gravity waves in the high-latitude ionosphere, *Journal of Geophysical Research*, *95*, 7693-7709.

Sangalli, L., D. J. Knudsen, M. F. Larsen, r. F. Pfaff, and D. Rowland (2008), Joule II Rocket-based measurements of ion velocity, neutral wind and electric field in the collisional transition region of the auroral ionosphere, *Journal of Geophysical Research*, *Under Review*.

Sauli, P. B., J. (2001), Tropospheric events and possible related gravity wave activity effects on the ionosphere, *Journal of Atmospheric and Solar-Terrestrial Physics*, *63*, 945-950.

Schulz, M. (2007), Magnetosphere, in *Handbook of the Solar-Terrestrial Environment*, edited by Y. Kamide and A. Chian, pp. 155-158, Springre-Verlag, Berlin Heidelberg.

Seker, I., J. D. Mathews, J. J. Makela, and D. J. Livneh (2008), Tracking F-region plasma depletion bands using GPS-TEC, Incoherent Scatter Radar, and All-Sky imager at Arecibo, *Journal of Atmospheric and Solar-Terrestrial Physics*, *Submitted*.

Seker, I., J. D. Mathews, J. Wiig, P. Farias-Gutierrez, J. S. Friedman, and C. A. Tepley (2007), First results from the Penn State Allsky Imager at Arecibo Observatory, *Earth Planets Science*, *59*, 165-176.

Sheen, D. R., and C. H. Liu (1988), Modeling F region gravity waves observed during the WAGS campaign, *Radio Science*, *23*, 894-904.

Shiokawa, K., Y. Otsuka, M. K. Ejiri, Y. Sahai, T. Kadota, C. Ihara, T. Ogawa, K. Igarashi, S. Miyazaki, and A. Saito (2002), Imaging observations of the equatorward limit of midlatitude traveling ionspheric disturbances, *Earth Planets Space*, *54*, 57-62.

Shiokawa, K., Y. Otsuka, C. Ihara, T. Ogawa, and F. J. Rich (2003), Ground and satellite observations of nighttime medium-scale traveling ionospheric disturbances at midlatitude, *Journal of Geophysical Research*, *108*, doi:10.1029/2002JA009639.

Shiokawa, K., Y. Otsuka, and T. Ogawa (2006), Quasiperiodic southward moving waves in 630-nm airglow images in the equatorial thermosphere, *Journal of Geophysical Research*, *111*, doi:10,1029/2005JA011406, 012006.

Sulzer, M. P. (1986), A radar technique for high range resolution incoherent scatter autocorrelation function measurements utilizing the full power of klystron radars, *Radio Science*, *21*, 1033-1040.

Tanimoto, T. (2005), The oceanic excitation hypothesis for the continuous oscillations of the Earth, *Geophys. J. International*, *160*, 276-288.

Tascione, T. F. (1994), *Introduction to the Space Environment*, 2 ed., Krieger, Malabar, Florida.

Taylor, M. J., J.-M. Jahn, S. Fukao, and A. Saito (1998), Possible evidence of gravity wave coupling into the mid-latitude F-region ionosphere during the SEEK campaign, *Geophysical Research Letters*, *25*, 1801-1804.

Thome, G. D. (1964), Incoherent Scatter observations of traveling ionospheric disturbances, *Journal of Geophysical Research*, *69*, 4047-4049.

Thome, G. D., and P. B. Rao (1969), Comparison of acoustic-gravity wave theory with UHF observations, *Final Report, 62 pp., Raytheon Co., Spencer Lab, Burlington, MA, May 1969*.

Tsugawa, T., Y. Otsuka, A. J. Coster, and A. Saito (2007), Medium-scale traveling ionospheric disturbances detected with dense and wide TEC maps over North America, *Geophysical Research Letters*, *34*, doi:10.1029/2007GL031663.

Vadas, S. L. (2006), Horizontal and Vertical Propagation, and Dissipation of Gravity Waves in the Thermosphere from Lower Atmospheric and Thermospheric Sources *Journal of Geophysical Research*, *Submitted*.

Vadas, S. L. (2007), Horizontal and Vertical Propagation, and Dissipation of Gravity Waves in the Thermosphere from Lower Atmospheric and Thermospheric Sources *Journal of Geophysical Research*, *112*, DOI: 10.1029/2006JA011845.

Vadas, S. L., and D. C. Fritts (2006), the influence of solar variability on gravity wave structure and dissipation in the thermosphere from tropopheric convection, *Journal of Geophysical Research*, *111, A10S12*, doi:10.1029/2005JA011510.

Villante, U., P. Di Giuseppe, and P. Francia (2003), On the correspondence between interplanetary, magnetospheric and geomagnetic fluctuations at selected frequencies, *Memorie-societa astronomica italiana*, *74*.

Wallace, J. M., and P. V. Hobbs (2006), *Atmospheric science: An introductory survey*, 2nd ed., Elsevier, Burlington; San Diego; London.

Wen, C.-H., D. J. Livneh, J. F. Doherty, and J. D. Mathews (2006), Pulse-Level Interference and Meteor Processing of Arecibo ISR data, *Journal of Atmospheric and Solar-Terrestrial Physics*, *69*, 973-980.

Zhang, S.-R., John M. Holt, Phil J. Erickson, Frank D. Lind, John C. Foster, Anthony P. van Eyken, Y. Zhang, Larry J. Paxton, William C. Rideout, Larisa P. Goncharenko, and Glenn R. Campbell (2005), October 2002 30-day incoherent scatter radar experiments at Millstone Hill and Svalbard and simultaneous GUVI/TIMED observations, *Geophysical Research Letters*, *32*.

Zhou, Q.-N., and J. D. Mathews (2006), On the physical explanation of the Perkins instability *Journal of Geophysical Research*, *in press*.

Zhou, Q.-N., J. D. Mathews, and C. A. Miller (2005), A preliminary investigation of the pseudo-spectral method numerical solution of the Perkins instability equations in the homogeneous case, *Journal of Atmospheric and Solar-Terrestrial Physics*, *67*, 325-335.

Zhou, Q.-N., J. D. Mathews, C. A. Miller, and I. Seker (2006), The evolution of nighttime mid-latitude mesoscale F-region structures: A case study utilizing numerical solution of the Perkins instability equations, *Planetary and Space Science*, *710-718*.

Vita

Ever since childhood, Dorey J. Livneh has been fascinated by science, engineering and mathematics. His interest in technical matters was aided by his parents, both of whom are engineers as they challenged the youngster to think about and explore these subjects. Upon graduating from Vincent Massey secondary school in Windsor, Ontario, Canada, he enrolled in the undergraduate Electrical Engineering program at the University of Western Ontario. After graduating, he declined to enter industry but instead chose the more interesting option of staying at UWO to work on meteor radar and earned Masters degree. Electing to pursue his budding interest in Aeronomy, he came to the Pennsylvania State University to complete his Ph.D. and write this dissertation.